Since January 2020 Elsevier has created a COVID-19 resource centre with free information in English and Mandarin on the novel coronavirus COVID-19. The COVID-19 resource centre is hosted on Elsevier Connect, the company's public news and information website.

Computers in Biology and Medicine 148 (2022) 105814

Contents lists available at ScienceDirect

Computers in Biology and Medicine

journal homepage: www.elsevier.com/locate/compbiomed

Identification of a novel immune-inflammatory signature of COVID-19 infections, and evaluation of pharmacokinetics and therapeutic potential of RXn-02, a novel small-molecule derivative of quinolone

Bashir Lawal [a,b,1], Yu-Cheng Kuo [c,d,1], Maryam Rachmawati Sumitra [a,b], Alexander T.H. Wu [e,f,g,h,*], Hsu-Shan Huang [a,b,h,i,j,**]

[a] PhD Program for Cancer Molecular Biology and Drug Discovery, College of Medical Science and Technology, Taipei Medical University and Academia Sinica, Taipei 11031, Taiwan
[b] Graduate Institute of Cancer Biology and Drug Discovery, College of Medical Science and Technology, Taipei Medical University, Taipei 11031, Taiwan
[c] Department of Pharmacology, School of Medicine, College of Medicine, Taipei Medical University, Taipei, 11031, Taiwan
[d] School of Post-baccalaureate Chinese Medicine, College of Chinese Medicine, China Medical University, Taichung, 40402, Taiwan
[e] The PhD Program of Translational Medicine, College of Medical Science and Technology, Taipei Medical University, Taipei 11031, Taiwan
[f] Clinical Research Center, Taipei Medical University Hospital, Taipei Medical University, Taipei, 11031, Taiwan
[g] TMU Research Center of Cancer Translational Medicine, Taipei Medical University, Taipei, 11031, Taiwan
[h] Graduate Institute of Medical Sciences, National Defense Medical Center, Taipei 11490, Taiwan
[i] School of Pharmacy, National Defense Medical Center, Taipei, 11490, Taiwan
[j] PhD Program in Drug Discovery and Development Industry, College of Pharmacy, Taipei Medical University, Taipei 11031, Taiwan

ARTICLE INFO

Keywords:
COVID-19 (Coronavirus disease 2019)
SARS-CoV-2 (severe acute respiratory syndrome coronavirus 2)
Pharmacokinetics
Immunomodulation
Inflammation

ABSTRACT

Coronavirus disease 2019 (COVID-19) is a global pandemic and respiratory infection that has enormous damage to human lives and economies. It is caused by SARS-CoV-2 (severe acute respiratory syndrome coronavirus 2), a non-pair-stranded positive-sense RNA virus. With increasing global threats and few therapeutic options, the discovery of new potential drug targets and the development of new therapy candidates against COVID-19 are urgently needed. Based on these premises, we conducted an analysis of transcriptomic datasets from SARS-CoV-2-infected patients and identified several SARS-CoV-2 infection signatures, among which TNFRSF5/PTPRC/IDO1/MKI67 appeared to be the most pertinent signature. Subsequent integrated bioinformatics analysis identified the signature as an important immunomodulatory and inflammatory signature of SARS-CoV-2 infection. It was suggested that this gene signature mediates the interplay of immune and immunosuppressive cells leading to infiltration-exclusion of effector memory T cells in the lungs, which is of translation relevance for developing novel SARS-CoV-2 drug and vaccine candidates. Consequently, we designed and synthesized a novel small-molecule quinoline derivative (RXn-02) and evaluated its pharmacokinetics in rats, revealing a peak plasma concentration (Cmax) and time to Cmax (Tmax) of 1.756 μg/mL and 0.6 h, respectively. Values of the area under the curve (AUC) (0–24 h) and AUC (0 h~∞) were 18.90 and 71.20 μg h/mL, respectively. Drug absorption from the various regional segments revealed that the duodenum (49.84%), jejunum (47.885%), cecum (1.82%), and ileum (0.32%) were prime sites of RXn-02 absorption. No absorption was detected from the stomach, and the least was from the colon (0.19%). Interestingly, RXn-02 exhibited *in vitro* antiproliferative activities against hub gene hyper-expressing cell lines; A549 (IC_{50} = 48.1 μM), K-562 (IC_{50} = 100 μM), and MCF7 (IC_{50} = 0.047 μM) and against five cell lines originating from human lungs (IC_{50} range of 33.2–69.5 μM). In addition, RXn-02 exhibited high binding efficacies for targeting the TNFRSF5/PTPRC/IDO1/MK signature with binding affinities (ΔG) of −6.6, −6.0, −9.9, −6.9 kcal/mol respectively. In conclusion, our study identified a novel signature of SARS-CoV-2 pathogenesis. RXn-02 is a drug-like candidate with good *in vivo* pharmacokinetics and hence

* Corresponding author. The PhD Program of Translational Medicine, College of Medical Science and Technology, Taipei Medical University, Taipei 11031, Taiwan.
** Corresponding author. Graduate Institute of Cancer Biology and Drug Discovery, College of Medical Science and Technology, Taipei Medical University, Taipei 11031, Taiwan.
E-mail addresses: chaw1211@tmu.edu.tw (A.T.H. Wu), huanghs99@tmu.edu.tw (H.-S. Huang).
[1] These authors contributed equally to this work.

https://doi.org/10.1016/j.compbiomed.2022.105814
Received 23 April 2022; Received in revised form 7 June 2022; Accepted 3 July 2022
Available online 11 July 2022

possesses great translational relevance worthy of further preclinical and clinical investigations for treating SARS-CoV-2 infections.

1. Introduction

Coronavirus disease 2019 (COVID-19) is a respiratory infection that has created a global pandemic which has produced enormous damage to human lives and economies [1,2]. It is caused by SARS-CoV-2 (severe acute respiratory syndrome coronavirus 2), a non-pair-stranded positive-sense RNA virus [3]. As of June 07, 2022, the COVID-19 pandemic has infected 535,601,240 people and claimed 6,320,955 lives according to an epidemiological report [4]. Similar to other fatal coronaviruses such as the SARS-CoV and MERS-CoV (Middle East respiratory syndrome coronavirus), SARS-CoV-2 activates a cascade of undue immune responses that can lead to multi-organ failure and death [5]. However, the death rates were reportedly high in old-aged patients and patients suffering from underlying diseases conditions such as high blood pressure, diabetes, cardiovascular disease, and other respiratory diseases [6,7].

The pandemic of COVID-19 is undergoing rapid evolution over time, with new viral strains appearing at frequent and regular intervals [8]. Among the various classes of SARS-CoV-2 variants, the delta and omicron variants collectively known as the Variant of Concern (VOC), are associated with significant changes in the behavior of the virus and its effect on the host [9]. Massive collaborative research all over the world on the viral structure, life cycle, properties, and functions has led to the development of several potent vaccines [10–15], with the aim of eliciting immunological responses by neutralizing antibodies (NAbs) against the SARS-CoV-2 spike protein [16], hence giving hope for an end to the era of the COVID-19 pandemic [3]. However, the emergence of the SARS-CoV-2 delta variant, and omicron variant in November 2021 in Botswana and South Africa [17,18], led to increased transmission and resistance to therapeutic monoclonal antibodies and vaccine-elicited antibodies [19]. Each of the SARS-CoV-2 variants has 10–15 mutations compared with the wild type [20], however, the omicron variant is described by the existence of about thirty-two (32) mutations in the receptor-binding and N-terminal domains of the spike protein which improve viral fitness and mediate antibody evasion [19].

Several computational and experimental studies [21,22], as well as clinical trials [19,23,24], were instigated to establish evidence around new investigational drug and vaccine candidates against viral infections. However, despite significant research efforts and available vaccines, effective therapeutics to limit the disease severity and mortality remain an unmet clinical need [25]. Therefore, the discovery and development of novel interventions strategies, including new drugs and vaccines that could avoid or alleviate the transmission and burden of SARS-CoV-2 infection have become a global health priority [26].

Among the various potential pharmacological targets, the ACE2 (angiotensin-converting enzyme 2) membrane receptor, RdRp (RNA-dependent RNA polymerase), TMPRSS2 (transmembrane protease serine 2), and PL^{pro} (papain-like protease) have been well explored for the development of potential drugs against COVID-19. Several antiviral drugs, including lopinavir, hydroxychloroquine, interferon, molnupiravir, and remdesivir, an RNA-dependent RNA polymerase (RdRp) inhibitor, have been used to treat COVID-19. However, the success of these drugs is limited by poor efficacy, safety concerns, and poor pharmacokinetic (PK) properties [27]. Molnupiravir, an orally administered *anti*-SARS-CoV-2 drug, has been reported to be well-tolerated, has oral bioavailability and good safety profile in humans [23,24]; however, its use is associated with risks of tumorigenesis, mutations in sperm precursor cell generation, and to embryo development [28]. Other drugs, including remdesivir, lopinavir, hydroxychloroquine, and interferon, had little or no effect on hospitalized patients with SARS-COV-2 infection as indicated by the initiation of ventilation, hospital stay duration, and overall mortality in interim World Health Organization (WHO) solidarity trial results [19]. This highlight the urgent need to expand and explore new drug targets as well as develop novel drug candidates for post-exposure targeted treatment of COVID-19.

Based on these premises, we conducted a comprehensive bioinformatics analysis using RNA sequencing datasets. We integrated differentially expressed genes (DEGs) from various transcriptomic datasets of SARS-COV-2 and identified CTLA3 (GZMA), TNFRSF5 (CD40), PTPRC (CD45), IDO1, and MKI67 (KI-67) as a novel biomarker signature for SARS-COV-2 pathogenesis which could be explored for targeted therapy. Subsequent integrated bioinformatics analysis suggested that this gene signature is associated with lung diseases, and mediates autoimmunity, and inflammatory and immune responses in SARS-CoV-2 infection. In addition, we report the design and development, PKs, and potential therapeutic efficacy of RXn-02 (10-chloro-6-(ethylamino)-12H-thiochromeno[2,3-quinolin-12-one), a novel small-molecule derivative of quinoline for treating SARS-CoV-2. We first evaluated the PK properties in a rat model, Next, we tested the potential of the drug for targeting the gene signature using *in silico* molecular docking studies. Interestingly, the drug exhibited good PKs and potential for targeting the signature with higher efficacy against the IDO1 protein. We also measured the antiproliferative activity of RXn-02 against cell lines expressing this gene signature. Collectively, this work has increased our understanding of the pathogenesis of COVID-19 and warrants in-depth evaluation of RXn-02 as a new therapy against SARS-CoV-2 infection via acting as a potential inhibitor of IDOI with the prospect of clinical translation.

1.1. Methods

1.1.1. Acquisition of SARS-CoV-2 transcriptomic data to identify a novel signature

The transcriptomic datasets of SARS-CoV-2 patients and healthy cohorts were acquired from the public domain database, the NCBI-GEO (Gene Expression Omnibus) microarray datasets. RNA expression profiles of patients and normal human control (no SARS-CoV-2 infection) were included (Table 1). The datasets were then analyzed for DEGs between infected and normal samples using the LIMMA package of R based on the log[fold change (FC)] selection cutoff points, adjusted *p*-value, and FDR (false discovery rate) of <0.05 [29]. The DEGs from each dataset were sorted and integrated to identify overlapping DEGs which were visualized using the online tool Multiple List Comparator.

1.2. Interaction and functional enrichment network analysis of the gene signature

The gene-gene interaction network of the novel gene signature was analyzed via the online gene interaction platform, GENEMANIA (https://genemania.org/) [30], while the protein-protein interaction (PPI) network of the gene signature was analyzed via the search tool for retrieval of interacting genes/proteins (STRING) server (http://string-db.org/, v10.5). PPI interactions were restricted to *Homo sapiens* depicted under default confidence (0.70) search and at a significance level of $p < 0.05$. Functional enrichment of the novel DEGs, including the Kyoto Encyclopedia of Genes and Genomes (KEGG) and gene ontology (GO) terms, was analyzed using Enrichr, an online gene set enrichment analysis (GSEA) server [31,32]. Enrichment analyses were conducted under a default enrichment cutoff value of $p < 0.05$. All enriched terms were visualized using the GO modules of ImageGP visualization tools.

Table 1
Characteristic of the microarray datasets of SARS-CoV2 patients used to identify the novel signature.

GSE-ID	Platform	SARS-COV-2	Control
GSE164571	GPL27956: NanoString Human nCounter PanCancer IO 360 Panel	5	2
GSE163529	GPL29514: NanoString GeoMx 2020 Broad COVID Platform	260	70
GSE159785	GPL29263: NanoString GeoMx Human Protein for nCounter 2020	6	3
GSE163530	GPL29514: NanoString GeoMx 2020 Broad COVID Platform	260	70
GSE159788	GPL29263; NanoString GeoMx Human Protein for nCounter 2020	99	99
	Datasets of the SARS-CoV-2 pathological hub gene validation of the signature		
GSE-ID	Organism	Remark	
GSE162208	*Mesocricetus auratus*	lung and blood of infected animals at different time points post infection	
GSE150847	*Mus musculus*	SARS-CoV-2 infected transduced human ACE2 mouse	
GSE162113	*Homo sapiens; Mus musculus*	expression changes of mouse organs with nCOV2 infection	
GSE158069	*Mus musculus*	SARS-CoV-2 infection in mice at different time	
GSE146074	*Mus musculus*	Mechanistic study of LY6E inhibits CoV entry into cells	
GSE148729	*Homo sapiens*	SARS-CoV-1/2 infected human cell lines	
GSE150392	*Homo sapiens*	Human iPSC-cardiomyocytes infected with SARS-CoV-2	
GSE156701	*Macaca mulatta*	SARS-CoV-2 Infected Humans and Rhesus Macaques	
GSE154613	*Homo sapiens*	transformed lung alveolar (A549) infected with SARS-CoV2	
GSE47961	*Homo sapiens*	SARS-CoV-2 Infected HAE cultures	
GSE162131	*Homo sapiens*	SARS-CoV-2 Infected human Nasal Epithelial Cells	

1.3. Drugs, reagents, and chemicals

The RXn-02 synthesis protocol is described below. A 10-mM stock solution of the drug was prepared in dimethyl sulfoxide (DMSO) and kept frozen at a temperature of −20 °C. Dulbecco's modified Eagle medium (DMEM) was obtained from Gibco-Invitrogen (Grand Island, NY, USA). All chemicals and organic solvents required for the synthesized reactions were purchased from either Sigma Aldrich Chemical (St. Louis, MO, USA) or Merck Chemical.

1.4. Cell lines and culture

Hub gene-expressing cell lines, including K-562, MCF-7, and A549, and four other human cell lines of lung origin, viz., HOP-62, NCI–H226, NCI–H322 M, and NCI–H522, were sourced from the US National Cancer Institute. Cells were cultured in DMEM supplemented with penicillin (25 U/mL), streptomycin (25 U/mL), and 10% fetal bovine serum (FBS) and incubated under 95% humidity, 37 °C in a 5% CO_2 condition. Cells were re-suspended in a fresh medium after 44–72 h and were sub-cultured at 75%–85% confluence.

1.5. In vitro antiproliferative assay

In vitro antiproliferative activities of RXn-02 against hub gene-expressing cell lines, including K-562, MCF-7, and A549 cells, and four other human cell lines of lung origin, viz., HOP-62, NCI–H226, NCI–H322 M, and NCI–H522 cells, were evaluated using the sulforhodamine B (SRB) reagent protocol [33]. About 5000–40,000 viable cells were seeded in each well of 96-well plates for 24 h. After 24 h of incubation, the medium was replaced, and cells were treated with RXn-02 at increasing concentrations of 0, 0.1, 1.0, 10, and 100 μM for 48 h. After incubation, cells were washed with 1% phosphate-buffered saline (PBS) and incubated with 10% trichloroacetic acid (TCA) at room temperature for 1 h [34]. The plates were washed with double-distilled (dd)H_2O, and further incubated with 0.4% SRB for 60 min. The plates were washed with 1% acetic acid to remove any unbound SRB dye. The plates were air-dried, and cells were re-dissolved in a 20 mM Tris-based solution for 15 min under constant agitation. Cell viabilities with different RXn-02 treatments were monitored at 515 nm. The 50% maximal inhibition of cell proliferation (GI_{50}) and the total growth inhibition (TGI) were calculated as described previously [35, 36].

1.6. In vivo PKs and in silico GastroPlus-Based simulation: parameter sensitivity assessment (PSA) analysis

Male albino Wistar rats (105.90 ± 4.25g, 6 weeks old) from BioLASCO (Taipei, Taiwan) and maintained under standard lab conditions (12-h light/dark cycle) at the Animal Center of Taipei Medical University. They were fed on a pelleted diet and water ad libitum and were allowed to acclimatize for one week. Animal experiments were approved by and conducted in strict compliance with the ethical conduct of Taipei Medical University as contained in the Affidavit of Approval (approval no. LAC-2017-0161). The rats were administered 5 mg/kg body weight (BW) of RXn-02 to determine its systemic PK parameters. A total of 24 blood samples were collected within the period of 24 h (1 h interval). Samples were collected in a disodium ethylenediamine tetra acetate (Na_2EDTA)-containing tube, centrifuged and processed to separate the plasma as described previously [37,38]. Samples were quantified for RXn-02 using a previously validated ultra-precision liquid chromatographic (UPLC) method [39]. The plasma concentration-time curve generated from the *in vivo* experiment was used to calculate the various PK parameters using the PKPlus™ module of GastroplusTM software (version 9.0, Simulations Plus Inc., Lancaster, CA, USA). The "peak plasma concentrations (Cmax), time to reach Cmax (Tmax) and area under the plasma concentration-time curve (AUC0-t) from time zero to the last measured concentration (Clast) were obtained from the plasma concentration-time curves. The rate constant (K) was calculated from the slope of the terminal phase of the log plasma concentration-time points. AUC from time zero extrapolated to infinity (AUC0→∞) was calculated as AUC0-t + Clast/K. In addition, the GastroPlusTM software based on the advanced compartmental absorption and transit (ACAT) model, was used to predict the regional drug absorption characteristics from nine gastrointestinal tracts (GIT) compartments, including the cecum, colon, stomach, jejunum-1, jejunum-2, duodenum, ileum-2, ileum-1, and ileum-3.

1.7. In silico analysis of the drug-likeness, metabolism, and permeability of RXn-02

We modelled and evaluated the drug-likeness, HIA (human intestinal absorption), and BBB (blood-brain barrier) permeability of RXn-02 using the SwissADME algorithm. BBB permeability was simulated using the BOILED EGG model of the algorithm. In addition, we explored the support vector machine_LiCABEDS algorithm model [40], and

mathematical calculations based on the molecular weight (MW) and number of H bonds to evaluate the BBB permeability of RXn-02 [41].

1.8. Molecular docking analysis

The three-dimensional (3D) crystal structures of the protein targets, namely, TNFRSF5 (PDB:1LB6), PTPRC (PDB:5FN6), IDO1 (PDB:4PK6), and MKI67 (PDB:1R21), were retrieved in protein data bank (PDB) format from the protein data bank and were converted to PDBQT format using AutoDock Vina software (vers. 0.8) [42]. The 3D structure of the ligand compound (RXn-02) was developed in MOL2 format using vers. 1.XX of the Avogadro molecular builder tool [43], and was subsequently converted to PDB format using the PyMOL Molecular Graphics System. The ligand (RXn-02) and receptors (target proteins) were prepared for the addition of hydrogen atoms (polar only), removal of water (H_20) molecules, and the addition of Kollman charges [44–46], prior to the docking simulation according to the methods described in previous studies [47,48]. Docking simulations were conducted using the default settings of AutoDock Vina (vers. 0.8). All bonds in the ligand rotated freely while considering the receptor to be rigid. A grid box of 40 × 40 × 40 Å at X, Y, and Z dimensions and a spacing of 1.0 Å were used. All docking was performed at exhaustiveness of 8 [36]. Docking complexes were visualized and analyzed for various interactions using the Discovery studio visualizer vers. 19.1.0.18287 (BIOVIA, San Diego, CA, USA) [49], and protein-ligand interaction profiler (PLIP) server.

1.9. Statistical analysis

All *in vitro* analyses were conducted in triplicate and analyzed using Graph-pad vers. 8.0. Data are presented as the mean ± SD (standard deviation). Statistical analysis of the results obtained was done via one-way analysis of variance (ANOVA) and the Tukey multiple ranges post-hoc Student's t-test was employed for statistical significance analysis between treatment doses. Data were considered statistically significant at $***p<0.001$, $**p<0.001$, $*p<0.05$.

2. Results and discussion

2.1. Transcriptomic identification of a novel biomarker signature of SARS-CoV-2 pathogenesis

We integrated DEGs from various SARS-CoV-2 datasets and identified a novel biomarker signature for targeted therapy. Based on the frequencies of gene occurrences from the SARS-CoV-2 databases, three clusters of DEGs were identified (Fig. 1A). The first cluster consisted solely of *CTLA3* (*GZMA*), the second cluster consisted of four genes including *TNFRSF5* (*CD40*), *PTPRC* (*CD45*), *IDO1*, and *MKI67* (*KI-67*), while the third cluster consisted of *B7–H3*, *BCLXL*, *ITGAX* (*CD11c*), *CD14*, *SCARI1* (*CD163*), *HCAM* (*CD44*), *NCAM* (*CD56*), *LAMP4* (*CD68*), and *EGFR* (Fig. 1A, B, and C). Further validation analysis of these signatures as a hub of pathological factors in SARS-CoV-2 cohorts revealed their significant roles in the pathology of various experimental and clinical SARS-CoV-2 infections (Fig. 1D). Altogether, our analysis of SARS-CoV-2 transcriptomic datasets identified new biomarker

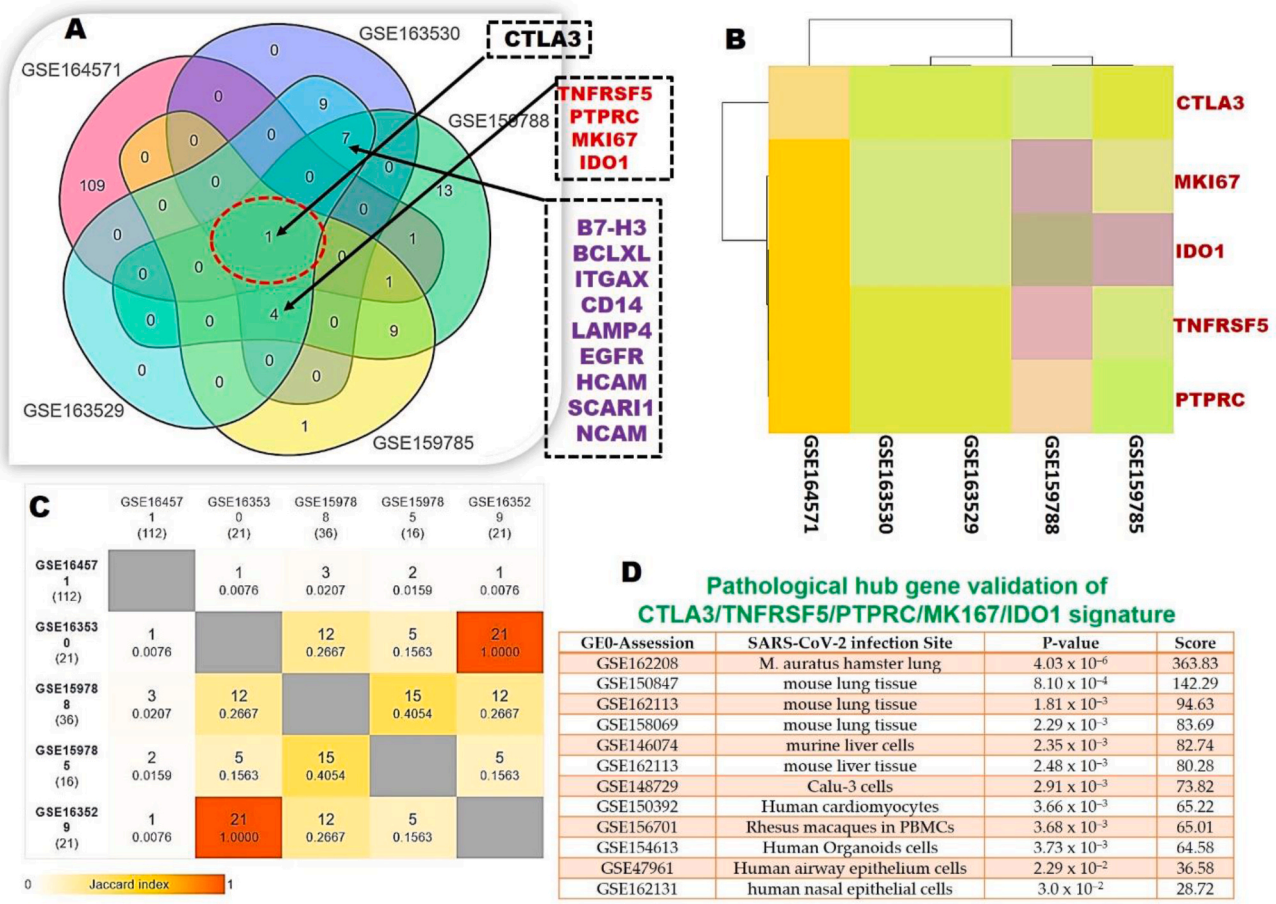

GE0-Assession	SARS-CoV-2 infection Site	P-value	Score
GSE162208	M. auratus hamster lung	4.03×10^{-6}	363.83
GSE150847	mouse lung tissue	8.10×10^{-4}	142.29
GSE162113	mouse lung tissue	1.81×10^{-3}	94.63
GSE158069	mouse lung tissue	2.29×10^{-3}	83.69
GSE146074	murine liver cells	2.35×10^{-3}	82.74
GSE162113	mouse liver tissue	2.48×10^{-3}	80.28
GSE148729	Calu-3 cells	2.91×10^{-3}	73.82
GSE150392	Human cardiomyocytes	3.66×10^{-3}	65.22
GSE156701	Rhesus macaques in PBMCs	3.68×10^{-3}	65.01
GSE154613	Human Organoids cells	3.73×10^{-3}	64.58
GSE47961	Human airway epithelium cells	2.29×10^{-2}	36.58
GSE162131	human nasal epithelial cells	3.0×10^{-2}	28.72

Fig. 1. Transcriptomic database identification of novel signatures for SARS-CoV-2. (A) Venn diagram of the DEGs identified based on log [fold change (FC)] integration of the DEGs from the SARS-CoV-2 datasets (B) Expression profiling of DEGs from each dataset (C) Heat map of the data associations from the datasets. (D) Pathological hub gene validation of the signatures in SARS-CoV-2 infections.

signatures that could be explored for SARS-CoV-2 targeted interventions.

2.2. Interactions and enrichment of the novel gene signature for SARS-COV-2

By utilizing the "STRING server, a database of known and predicted protein-protein interactions, based on physical and functional associations from knowledge transfer between organisms, and from interactions aggregated from other databases" [50], we found that the protein-protein interaction of the signature achieved the enrichment p-value of <1.0e-16, and generated 17 nodes, 62 edges, with an average node degree of 7.29 and average local clustering coefficient of 0.729 (Fig. 2A). GeneMANIA is an online interaction server that predicts the interactions and functions of a gene set. It finds other genes that are related to a set of input genes, using a very large set of functional association data including the protein and genetic interactions, co-localization, co-expression, pathways, and protein domain similarity [30]. Interestingly, our GGI network analysis based on the GeneMania database revealed enrichment in several immunological responses associated with neuroinflammatory response, T cell and leukocyte proliferation (Supplementary file). Furthermore, the enrichment analysis of the gene signature via the Enrichr server, an online gene set enrichment analysis (GSEA) server [31,32] revealed that the gene signature is enriched in several KEGG pathways; NF-kappa B signaling, asthma, the intestinal immune network for the production of IgG, primary immunodeficiency, autoimmune thyroid disease, transcriptional misregulation in cancer, Epstein-Barr virus infection, adherens junction, NSCLC, and PD-L1 expression and PD-1 checkpoint pathway (Fig. 2B, and C), while the enriched biological process included the regulation of protein kinase C activity, nitric oxide-mediated signal transduction, lymphocyte aggregation and apoptotic processes, TRIF-dependent toll-like receptor signaling, CD40 signaling, dendritic cell antigen processing and presentation, NIK/NF-kappaB signaling and immune response-regulating cell surface receptor signaling pathway. Interestingly, our analysis of human phenotypes ontologies identified the role of the signature mainly in the immune response and lung disorders: IgG deficiency, alveolar cell carcinoma, neoplasma of the lung, tracheobronchial and respiratory system (Fig. 2D). Collectively our PPI network and enrichment analysis strongly suggest the involvement of the

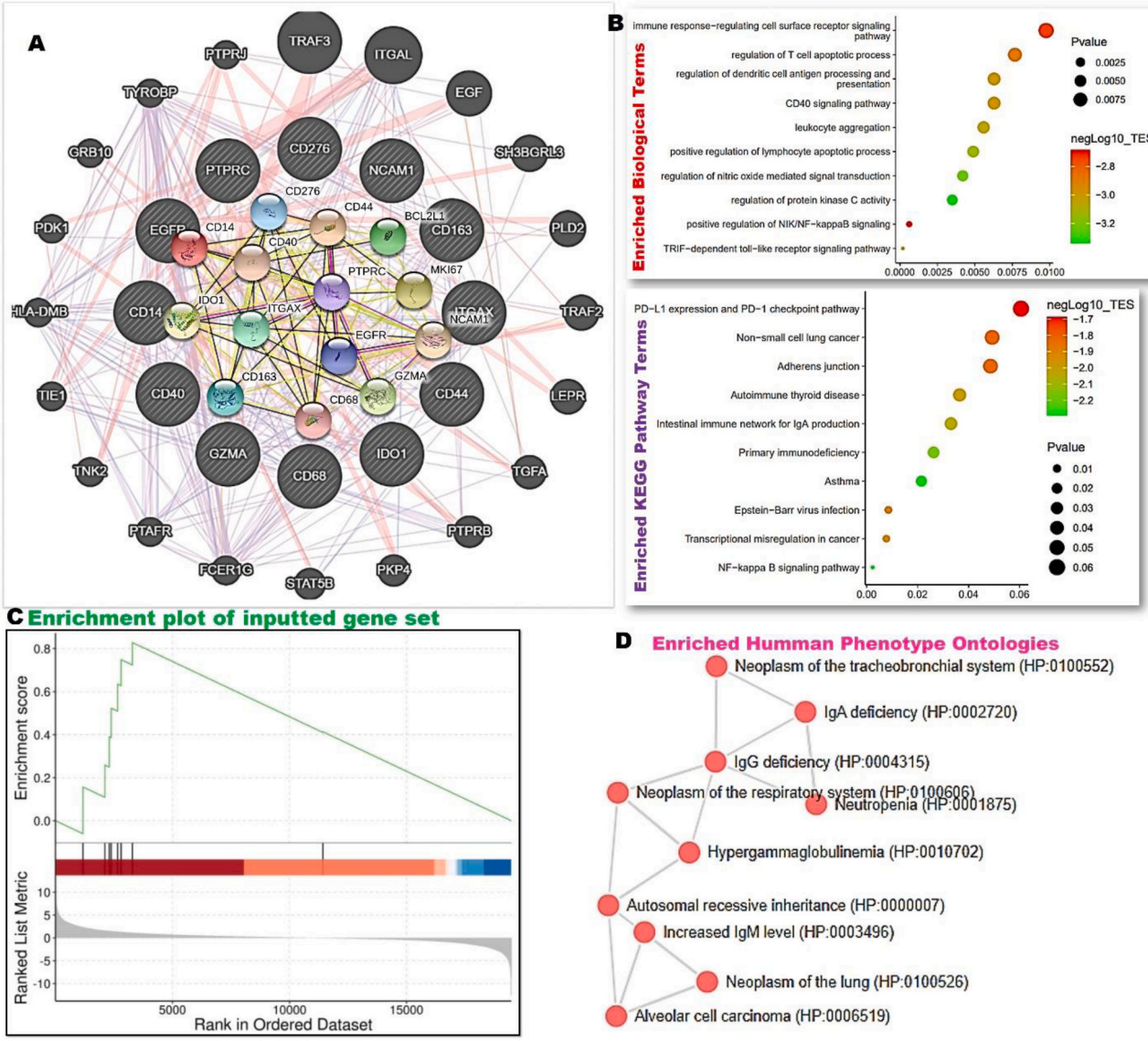

Fig. 2. Interactions and enrichment of the novel gene signature for SARS-COV-2. (A) The Gene-gene and protein-protein interaction networks of the hub gene signature of COVID-19 infection. (B and C) The enriched biological process and KEGG pathways of the hub gene signature. (D) Enriched human phenotypes ontologies of the hub gene signature.

signature in mediating infections, immunological and inflammatory response in the lungs, and hence the possible role of the signature in the pathology of SARS-COV2 infection.

2.3. Biomedical and clinical mapping suggested hub gene involvement in inflammatory and immune responses and identified cell line models for exploration of therapies against COVID-19 infection

We conducted biomedical and clinical mind mapping of hub genes and identified several network connections based on verified data: *TNFRSF5* (22,742 connections), *GZMA* (5393 connections), *IDO1* (10,942 connections), *MKI67* (11,364 connections), and *PTPRC* (19,594 connections). The most significant clinical mapping associations are summarized in Fig. 3. Clinical mapping of cell line expressions identified HeLa, K-562, MCF-7, and A549 cells as hub-gene-expressing cell lines, which could be explored as models for therapeutic targeting of hub genes. Interestingly, the hub gene co-expression analysis identified several inflammatory and immunoregulatory genes including *NFκB1*, *RELA*, *CD83*, *NDUFA2*, *CD14*, *CD34*, *CD86* and *CD80*, that were associated with the roles of the hub genes in the pathology of COVID-19 infections. In addition, the biology of the hub genes was mainly related to T-cell activities, cell proliferation, and immune responses. Altogether, clinical mapping of the hub genes suggested the strict involvement of these genes in regulating inflammatory and immune responses during COVID-19 infection. Hence, they could serve as novel targets for treating COVID-19.

2.4. The gene signature was suggested to mediate the interplay of immune and immunosuppressive cells leading to infiltration-exclusion of effector memory T cells in the lungs; translation for the development of novel SARS-CoV-2 drug and vaccine candidates

SARS-CoV-2, just like other fatal coronaviruses (SARS-CoV and MERS-CoV) mitigate a cascade of undue immune responses that can lead to the failure of the various organs and death [5]. However, the understanding of immunity to SARS-CoV-2 is improving along with the development of candidate drug and vaccine interventions [51]. Herein, we evaluated the role of the gene signature of SARS-CoV-2 in immune infiltrations of the lungs. Based on the immune infiltration of the gene signature, we found that the most abundant MKi67-induced infiltrating cells were the T helper type 1 (Th1), induced regulatory T cells (iTregs), and natural (n)Tregs suggesting that Tregs are the most likely cells that may be associated with role of MKi67 in SARS-CoV-2 pathogenesis in the lungs. On a contrary note, cytotoxic T cells, macrophages, natural killer (NK) cells, iTregs, Th1 cells, and follicular helper T (Tfh) cells, were the most abundant cells that infiltrated the lungs in the presence of high IDO1, PTPRC, and CD40 expressions (Fig. 4A). These findings strongly suggest that the pathogenic role of the SARS-CoV-2 novel signature is

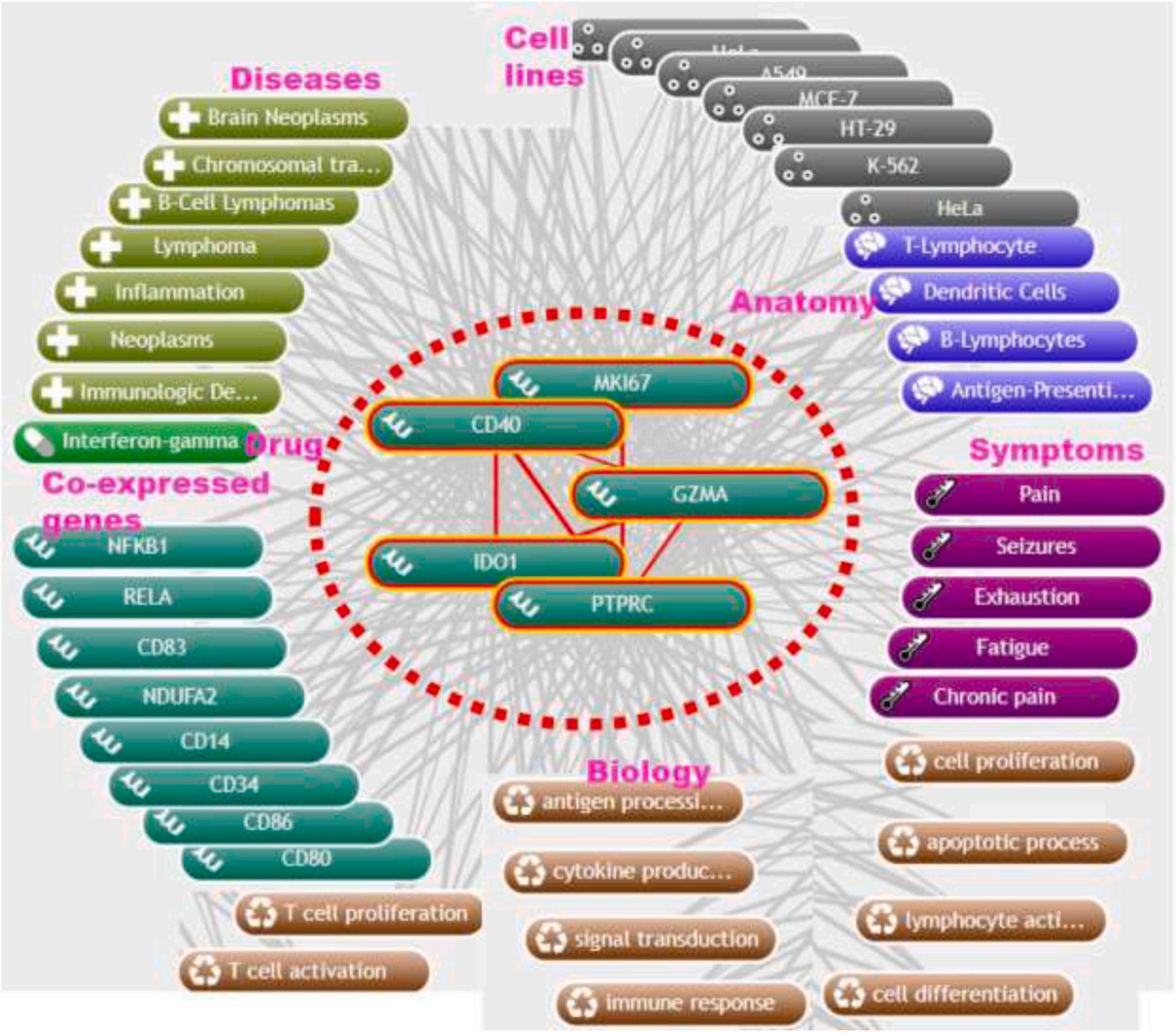

Fig. 3. Plot of biomedical and clinical mind mapping of hub genes based on verified data: *TNFRSF5* (22,742 connections), *GZMA* (5393 connections), *IDO1* (10,942 connections), *MKI67* (11,364 connections), and *PTPRC* (19,594 connections).

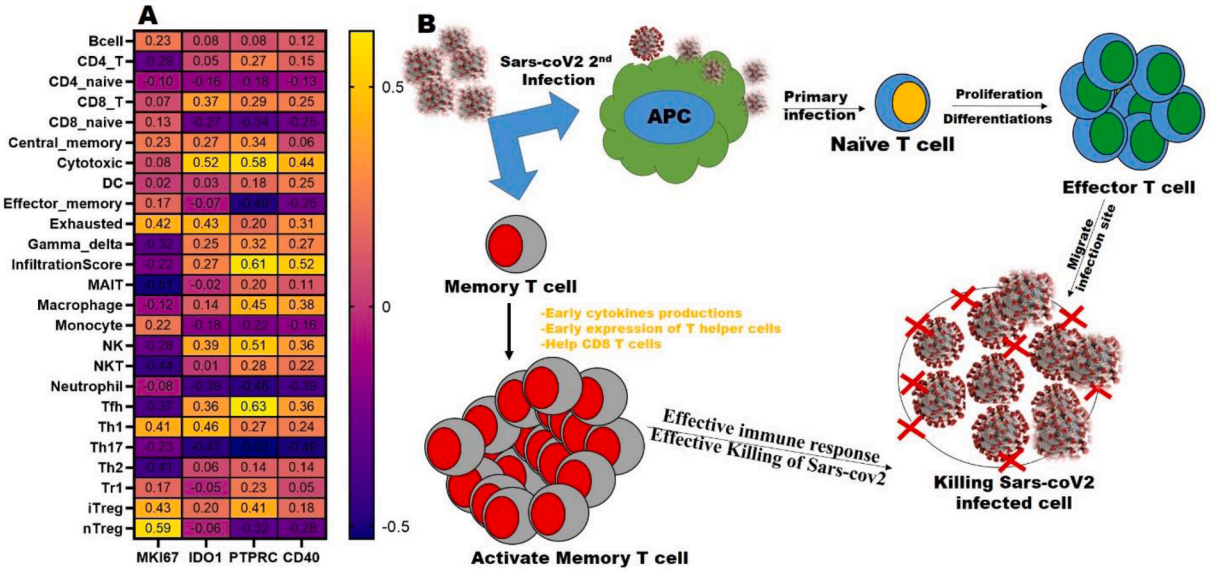

Fig. 4. The gene signature was suggested to mediate the interplay of immune and immunosuppressive cells leading to infiltration-exclusion of effector memory T cells in the lungs. (A) Gene signature expression correlations with the infiltration of immunosuppressive and immune cells in the lungs. (B) Effector memory T cells during primary and secondary SARS-CoV-2 infections.

associated with the interplay between immune and immunosuppressive cells that infiltrate into the lungs. This interplay of immune and immunosuppressive cells within the lungs of SARS-CoV-2 novel signature expression, however, was found to lead to the infiltration-exclusion of effector memory T cells, monocytes, neutrophils, and Th17 cells. Th17 cells are a pro-inflammatory subset of T helper cells responsible for the production of interleukin (IL)-17 [52]. Th17 cells have an important function in adaptive immunity by protecting the body against pathogens [53]. They exhibit protective and non-pathogenic roles by maintaining mucosal barriers and aiding pathogen clearance at mucosal surfaces [52,53]. Effector memory T cells play a vital role in immunity against pathogenic agents [54]. Effector cells are short-lived cells, while memory cells are long-lived survival-memory cells. When a pathogenic antigen is presented to naive T cells by antigen-presenting cells, the T cells become activated, proliferate, and differentiate into effector cells which move to the infection site to eliminate the pathogen [55]. Consequently, during re-exposure to an antigen, a secondary immune response is activated, and memory T cells undergo rapid expansion, secrete high-affinity neutralizing antibodies, and cause more-effective immune responses (Fig. 4B) and pathogen elimination [55,56]. These effector memory T cells have potential relevance for effective immunity against SARS-CoV-2 infection [57], and hence the exclusion of infiltration by these effector memory T cells can be attributed to increased cases of SARS-CoV-2 re-infection after having received vaccinations [58–62]. Altogether, our study sheds more light on SARS-CoV-2 pathogenesis and identifies a novel signature target with translational relevance for developing novel SARS-CoV-2 drug and vaccine candidates.

2.5. Rationale for the structurally guided pharmacophore hybridization strategy for the design of RXn-02

Pharmacophore hybridization and hopping of bioactive compound scaffolds are important approaches for the design and development of novel drugs [63]. Quinolines and their derivatives play important roles in heterocyclic chemistry due to their various biological activities, including antioxidant [64], *anti*-plasmodial [65], anti-inflammatory [66], anticancer [67], antibacterial [68], and antiviral properties [69,70], as well as several other biological activities [71]. Hydroxy-chloroquine (HCQ) and chloroquine (CQ) are quinoline-based antiplasmodial drugs with repurposing potential for treating COVID-19. Several *in silico*, *in vitro, in vivo*, and clinical studies have reported the efficacy of chloroquine for treating SARS-CoV-2 infections [72–78], and it has received US Food and Drug Administration (FDA) authorization for compassionate use in COVID-19 patients. In addition to reducing the viral load, chloroquine also exhibited anti-inflammatory [79], anti-proliferative [80], and immunomodulatory [81] activities. In addition, several other anti-inflammatories, anti-proliferative and immunomodulatory drugs, including camptothecin, irinotecan, and topotecan, contain quinolones as their major backbone responsible for their biological activities [82,83].

The thiochromeno moiety is a privileged structure in modern medicinal chemistry, especially in the discovery of new anti-cancer, anti-angiogenic, and anti-infectious agents [84,85]. Due to the importance of thiochromeno, we directed our efforts toward developing its derivatives to treat COVID-19 infections. Therefore, due to the various activities mentioned above, these compounds (quinoline and thiochromeno) and their derivatives may represent target compounds worthy of preclinical evaluation and future clinical trials for treating COVID-19. In the present study, we developed RXn-02 (Fig. 5), a hybridized novel small molecule using structurally guided pharmacophore hybridization and scaffold hopping of these bioactive compounds from natural products (quinoline) and thiochromeno. RXn-02 (10-chloro-6-(ethylamino)-12 H-thio--chromeno[2,3-*c*]quinolin-12-one) was synthesized using isatin as the starting material via several patented protocols [86–88].

2.6. In vivo PK properties of RXn-02

Determining the PK properties of a drug is an integral part of early drug discovery and development. It is an important feature that defines the clinical success of a therapeutic agent [89,90]. Many drugs fail in clinical trials due to poor PKs [91–93]. Based on this premise, we evaluated the drug-likeness and PKs of RXn-02 using *in silico* studies and *in vivo* animal models. Plasma concentration-time profiles of RXn-02 after administration and its PKs are presented in Fig. 6**.** Values of the peak plasma concentration (Cmax) and time to reach Cmax (Tmax) were found to be 1.756 μg/mL and 0.6 h, respectively, when administered orally. Values of the AUC (0–24) and AUC (0∼∞) after oral administration were 18.90 and 71.20 μg h/mL, respectively. GastroPlusTM simulation and prediction software is the most advanced and reliable method of determining the amount of drug absorbed from the nine

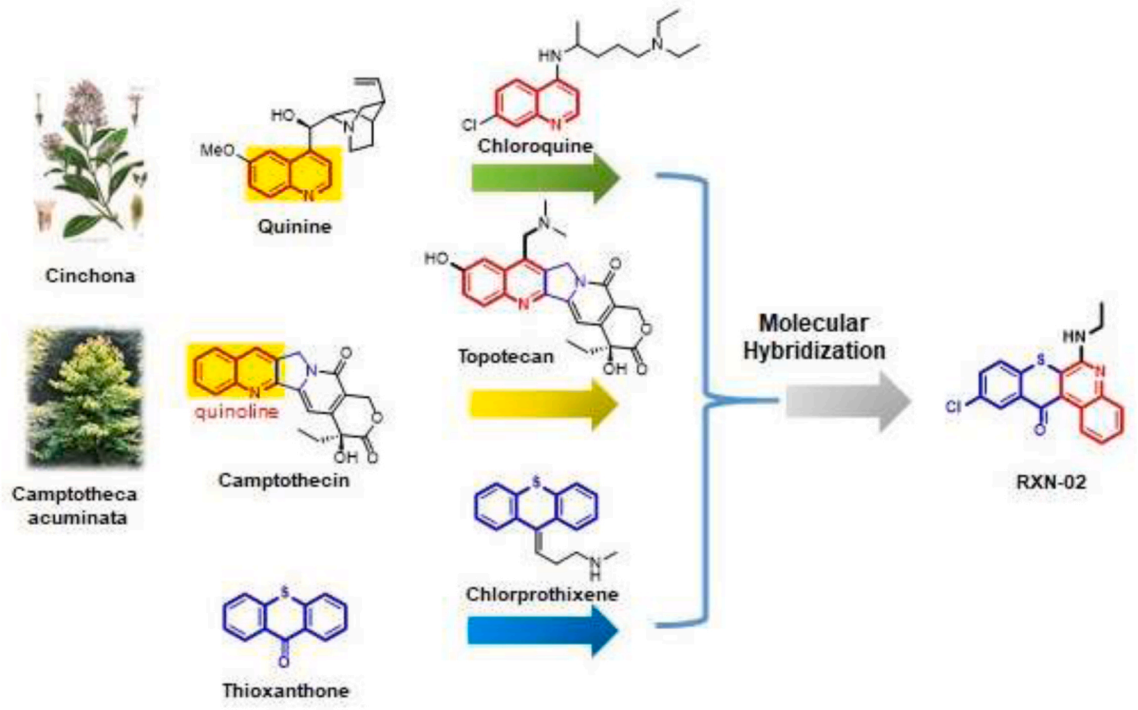

Fig. 5. Rationale for the structurally guided pharmacophore hybridization strategy for designing RXn-02 (10-chloro-6-(ethylamino)-12H-thiochromeno[2,3-c] quinolin-12-one).

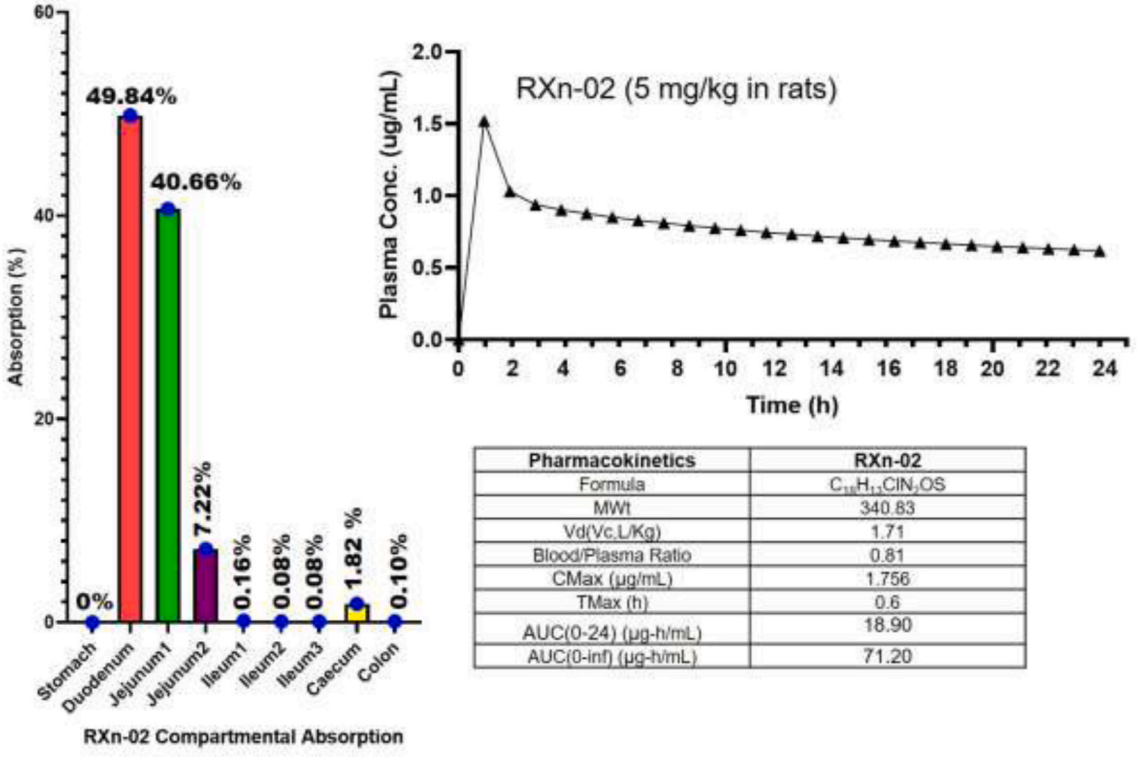

Pharmacokinetics	RXn-02
Formula	$C_{16}H_{11}ClN_2OS$
MWt	340.83
Vd(Vc,L/Kg)	1.71
Blood/Plasma Ratio	0.81
CMax (μg/mL)	1.756
TMax (h)	0.6
AUC(0-24) (μg-h/mL)	18.90
AUC(0-inf) (μg-h/mL)	71.20

Fig. 6. Pharmacokinetic parameters of orally administered RXn-02. Cmax, maximum concentration in plasma; Tmax, time to reach Cmax; AUC, area under plasma concentration-time curve.

segments of the GIT. Values of the drug absorption from the various regional segments are illustrated in Fig. 6. The duodenum (49.84%), jejunum (47.88%), cecum (1.82%), and ileum (0.32%) were prime sites of RXn-02 absorption. The least absorption occurred in the colon (0.19%), and no absorption was detected in the stomach.

2.7. Drug likeness, membrane permeation, and metabolism of RXn-02

RXn-02 was found to satisfy the criteria of drug-like candidates based on the Lipinski rule. High topological polar surface area (TPSA) (70.23), human intestinal absorption (HIA), and bioavailability (>50%) suggested its good permeation of various biological barriers (Fig. 7A). In addition, RXn-03 was able to permeate the BBB and was not a substrate for P-glycoprotein 1 (P-gp) or multidrug-resistance protein 1 (MDR1), which pumps drugs and various compounds out of cells [94]. These findings suggest the good absorption, permeability, retention, and optimal drug delivery of RXn-02 [95]. Inhibition of CYP450 isoforms, a group of drug-metabolizing isozymes, may lead to inhibition of a drug's biotransformation and induce drug-drug interactions in which co-administered drugs accumulate to toxic levels [96,97]. Among the various isoforms of CYP450, we found that RXn-02 is a substrate for CYP1A2, CYP2C9, and CYP3A4 (Fig. 7B and C). CYP1A2 is localized to the endoplasmic reticulum, while CYP3A4 is mainly found in the liver and intestines [98]. CYP2C9 on the other hand is mainly expressed in the liver, duodenum, and small intestine [99], and makes up about 18% of the cytochrome P450 protein in liver microsomes [99]. Our findings are in line with our *in vivo* results which demonstrated that the duodenum (49.84%) was the major site for RXn-02 absorption. The presence of these isoforms in the liver, duodenum, and small intestine indicates that these organs are sites of clearance of RXn-02.

2.8. RXn-02 demonstrated in vitro antiproliferative properties against hub gene hyper-expressing cell lines and cell line subsets of human lung origin; translational relevance for treating SARS-CoV-2 infection

The severity of COVID-19 complications can be attributed to increased expression levels of TMPRSS2, ACE2 and hub genes in overactively dividing cells, leading to compromised immune responses and a worse prognosis of COVID-19 infection. It is therefore of utmost significance to evaluate therapeutic approaches against SARS-CoV-2 using experimental models that reiterate aspects of the human disease [26]. On this premise, therapeutic agents with anti-proliferative effects against cell lines originating from the human lungs would be useful in treating or alleviating COVID-19 infections. Based on this premise, we evaluated the anti-proliferative activities of RXn-02 against five subsets of human lung cell lines. Interestingly, RXn-02 exhibited dose-dependent anti-proliferative activities against hub gene hyper-expressing cell lines including A549, K-562, and MCF7 with IC_{50} values of 48.1, 100, and 0.047 μM respectively (Table 2). In addition, RXn-02 demonstrated its activity against all five cell lines originating from human lungs with an IC_{50} range of 33.2–69.5 μM. These cell lines exhibited high expression levels of the signature (TNFRSF5, PTPRC, IDO1, and MKI67). Therefore, by translation, the anti-proliferative effects of RXn-02 on these cell lines strongly suggested its potential for decreasing the risk of SARS-CoV-2 infection and its severe complications. Altogether, our study points out the potential role of RXn-02 in preventing and treating COVID-19 infection.

Values are from triplicate determination ($n = 3$) of the mean optical densities (SD ± 0.02). * $p < 0.05$, ** $p < 0.01$, and *** $p < 0.001$ significantly differ compared to the untreated control.

2.9. Exploring the potential of RXn-02 for targeting the TNFRSF5/PTPRC/IDO1/MKI67 signature

Molecular docking is a widely explored simulation tool for modeling the potential binding efficacy of a small-molecule drug candidate and its targeted protein molecules, and for evaluating interactions between the protein-ligand docked complex [89,100–102], thus providing insights into the biological activities of the drug candidate and aiding drug discovery and development [103–107].

RXn-02_IDO1 docking complex: Consequently, our molecular docking analysis revealed that RXn-02 is bound to IDO1 with the highest binding affinity (ΔG) of −9.9 kcal/mol (Fig. 8). RXn-02 is bound to IDO1 by a single hydrogen bond with His 346(3.24) residues of the IDO1-

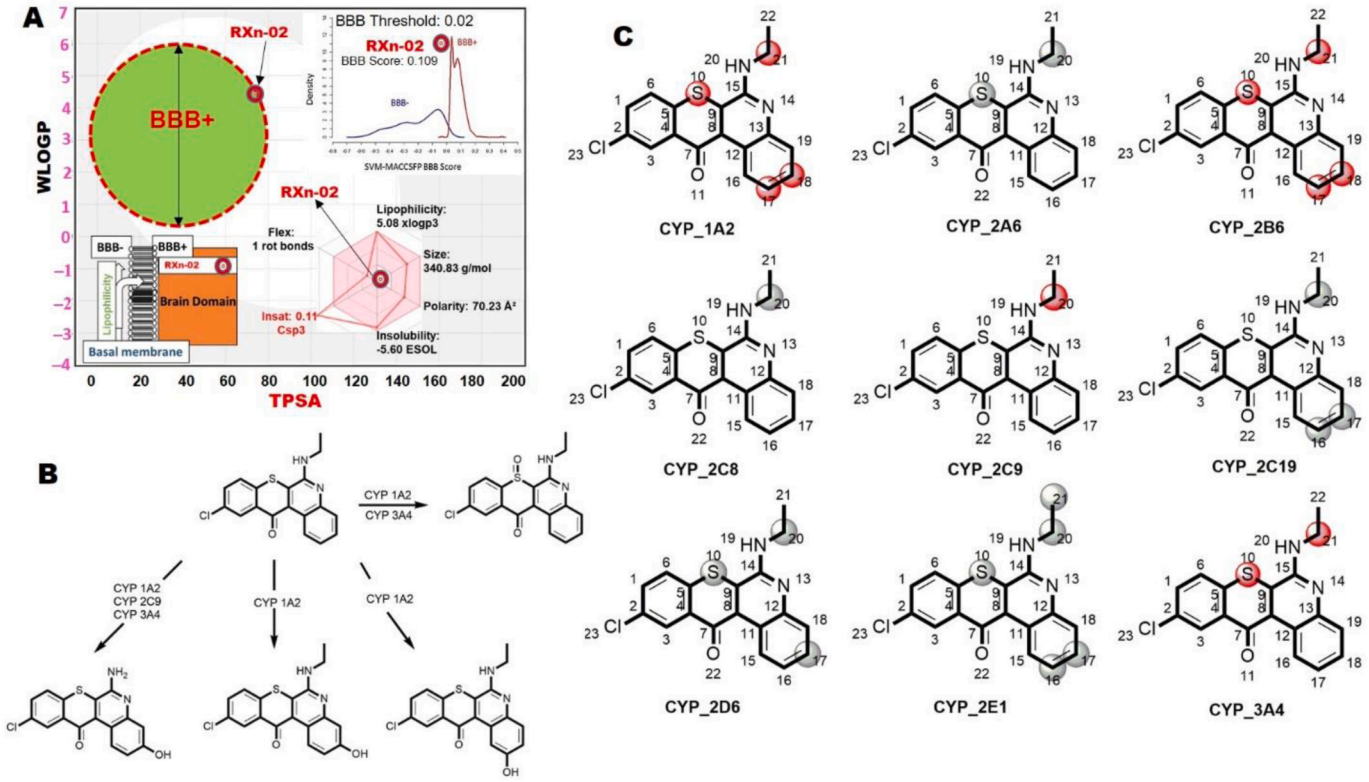

Fig. 7. (A) Drug likeness, membrane permeation, and (B, C) metabolism of RXn-02.

Table 2
In vitro activities of RXn-02 against hub gene hyper-expressing cell lines and cell line subsets of human lung origin.

		RXn-02 (μM)						
	Cell line	Ctrl	0	0.1	1.0	10	100	IC_{50} (μM)
Hub gene hyper-expressing cell lines	A549	2.039	2.059	1.997	1.883	1.602**	1.129**	48.1
	K-562	1.681	1.787	1.771	1.668	1.242	1.056*	100
	MCF7	2.250	1.855	1.083	0.873	0.735***	0.699***	0.047
Human cell lines of human lung origin	HOP-62	1.883	1.841	1.859	1.761	1.463*	0.319***	13.3
	NCI–H226	2.573	2.446	2.389	2.367	2.142*	1.704**	33.2
	NCI–H322 M	1.501	1.445	1.491	1.386	1.209*	1.020*	69.5
	NCI–H522	2.408	2.387	2.405	2.362	2.110*	1.395**	24.8
	A549/ATCC	2.039	2.059	1.997	1.883	1.602**	1.129**	48.1

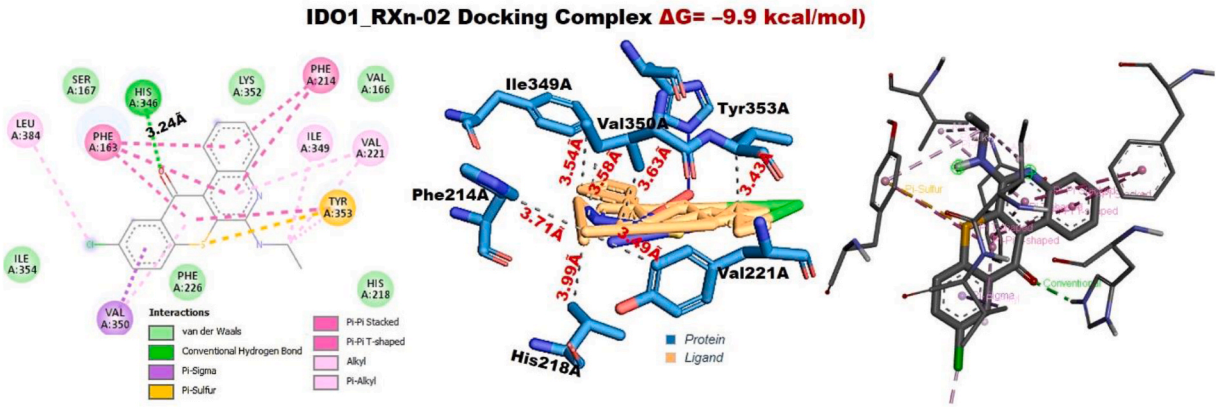

Fig. 8. Ligand receptor interaction simulation of RXn-02 withindolamine 2,3-dioxygenase 1 (IDO1). Two-dimensional view of the IDO1-RXn-02 complex showing interacting amino acids and interaction distances of hydrogen bonds between the receptor and ligand (left panel). The right panel displays hydrophobic contacts occurring between RXn-02 and IDO1.

binding domain. Several pi-interactions, including p-pi stacking (Phe16, and Phe214), pi-sigma (Val350) pi-pi T shape (Tyr353), and p-alkyl (Leu384, Ile349, and Val221), were found within the RXn-02_IDO1 complex. These high numbers of pi interactions may be attributed to the higher binding efficacy of RXn-02 towards IDO1 compared to its affinity for other targets. In addition, the RXn-02_IDO1 complex was enriched with six Van der Waals forces (Ser167, Ile354, Phe2256, Lys352, Val166, and His218) and several hydrophobic contacts with Phe214A (3.71 Å), His218A (3.99 Å), Ile349A (3.54 Å), Val350A (3.58 Å), Val221(3.49 Å), and Tyr353A (3.43 Å).

MKi67_RXn-02 docking complex: RXn-02 is bound to MKi67 with a binding affinity (ΔG) of −6.9 kcal/mol, and a binding proximity range of 2.49 Å in hydrogen bonds with Arg5 and Leu22 residues of the MKI67-binding domain. Four alkyl interactions (Ile53, Arg6, Pro21, and Pro3) van der Waals forces (Trp2 and Met01), and five hydrophobic contacts with Thr44A (3.94 Å), Arg5A (3.65 Å), Pro21A (3.90 Å), Leu22A (3.33 Å), and Ile53A (3.77 Å) placed MKi67 as the second most preferred target for RXn-02 ligand-binding ability (Fig. 9).

TNFRSF5_RXn-02 docking complex: RXn-02 is bound to TNFRSF5 with a binding affinity (ΔG) of −6.6 kcal/mol, and a binding proximity range of 2.08–2.32 Å in hydrogen bonds with Arg402, Gln396, and Cys403 residues of the TNFRSF5-binding domain. In addition, alkyl (Ile607, Phe609, Val474, His394), pi-sigma (Ala400), and pi-sulfur (Cys403) interactions were found for the TNFRSF5 and RXn-02 docked complex. Several van der Waals forces with Gln605, Thr399, Gln401, Phe410, Ser408, and Leu397, and hydrophobic contacts with Al400A (3.98 Å), Arg402A (3.68 Å), Val474A (3.19 Å), Ile607B (3.79 Å), and Phe609B (3.74 Å) were found intercalated with RXn-02 within the TNFRSF5 cavity (Fig. 10).

RXn-02_PTPRC docking complex: RXn-02 demonstrated the least

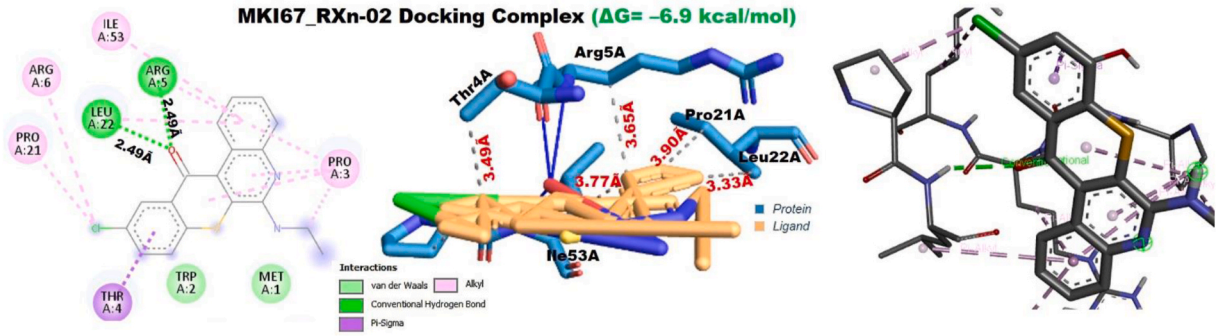

Fig. 9. Ligand receptor interaction simulation of RXn-02 with marker of proliferation Ki-67 (MKi67). Two-dimensional view of the MKi67-RXN-02 complex showing interacting amino acids and interaction distances of hydrogen bonds between the receptor and ligand (left panel). The right panel displays hydrophobic contacts occurring between RXn-02 and MKi67.

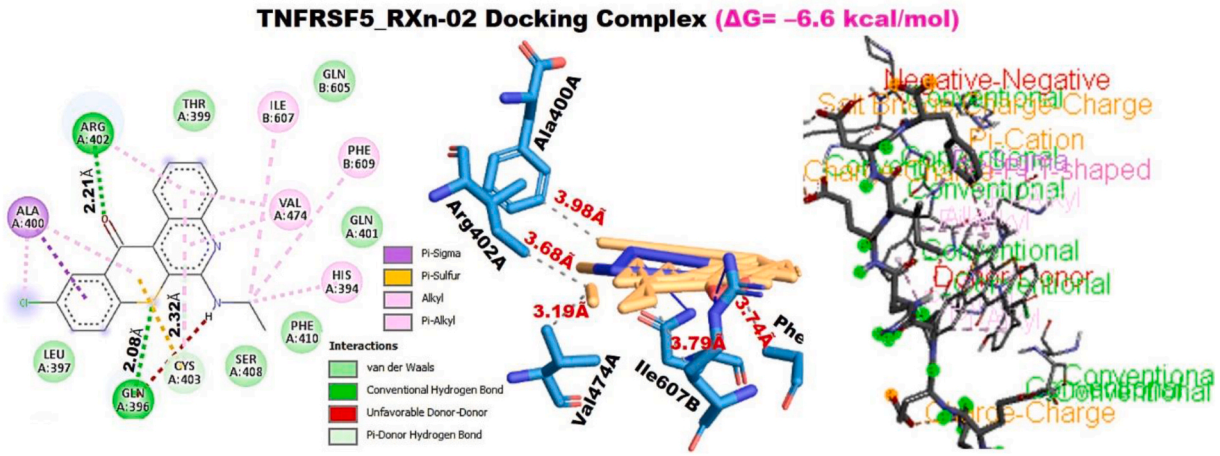

Fig. 10. Ligand receptor interaction simulation of RXn-02 withtumor necrosis factor receptor superfamily member 5 (TNFRSF5). Two-dimensional view of theTNFRSF5_RXn-02 complex showing interacting amino acids and interaction distances of hydrogen bonds between the receptor and ligand (left panel). The right panel displays hydrophobic contacts occurring between RXn-02 andTNFRSF5.

binding affinity (ΔG of −6.0 kcal/mol) and molecular interactions towards the binding domain of PTPRC. Although three hydrogen bonding interactions (Ser174 (2.59 Å), Asp101 (2.39 Å), and Thr102 (3.05 Å)) were engaged in the docked complex, the fewer alkyl interactions (Val250, Arg252, and Lys99), van der Waals forces (only Gly173, Glu98, Gln251, and Pro144), and hydrophobic contacts made PTPRC a less-favourable target for RXn-02 ligand-binding ability (Fig. 11).

Altogether, our molecular docking analysis hinted at the translational therapeutic role of RXn-02 for treating SARS-CoV-2 infection via targeting the TNFRSF5, PTPRC, IDO1, and MKI67 signatures. However, further preclinical studies to evaluate the direct effect of RXn-02 on the SARS-CoV-2 virus are required.

3. Conclusions

The present study leveraged the transcriptomic datasets from SARS-CoV-2-infected patients and identified a novel immune-inflammatory signature of SARS-CoV-2 infection. This gene signature was suggested to mediate the infiltration-exclusion of effector memory T cells in the lungs. RXn-02, a novel small molecule derivative of quinoline demonstrated good drug-likeness, pharmacokinetics properties, and translational relevance for the treatment of SARS-CoV-2 infection.

Data availability statement

Data supporting the results of this manuscript will be made available, without undue reservation.

Conflicts of interest

No conflict of interest.

Funding

H-SH was funded by the Ministry of Science and Technology (MOST111-2314-B-038-017 and MOST111-2314-B-038-122), Taiwain. A.T.H.W was funded by the Ministry of Science and Technology (111-2314-B-038 -142 and 111-2314-B-038 -098), Taiwan.

Author contributions

All authors contributed to the study design, analysis, data collections, writing, editing and approving the final version of the manuscript.

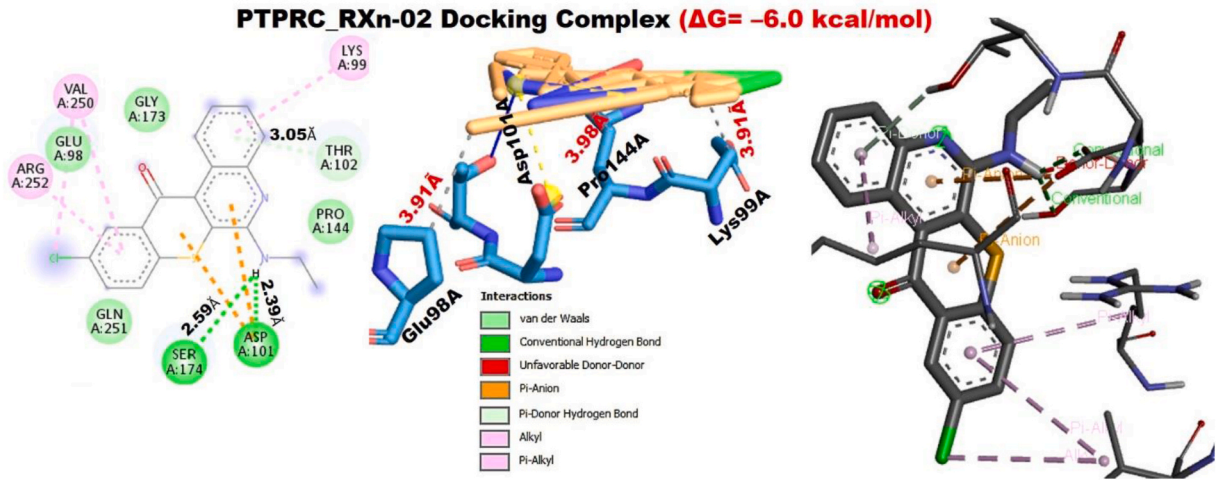

Figure 11. Ligand receptor interaction simulation of RXn-02 withprotein tyrosine phosphatase receptor type C (PTPRC). Two-dimensional view of the PTPRC-RXN-02 complex showing interacting amino acids and interaction distances of hydrogen bonds between the receptor and ligand (left panel). The right panel displays hydrophobic contacts occurring between RXn-02 and PTPRC.

Declaration of competing interest

The authors declare no conflicts of interest.

Appendix A. Supplementary data

Supplementary data to this article can be found online at https://doi.org/10.1016/j.compbiomed.2022.105814.

References

[1] P.A. Leggat, J. Frean, L. Blumberg, COVID-19: current challenges and future perspectives, Multidisciplinary Digital. Pub. Insitute. 7 (2022) 16, https://doi.org/10.3390/tropicalmed7020016.

[2] A. Kumar, COVID-19 current challenges and future perspectives, Bentham Sci. Pub. (2021), https://doi.org/10.2174/9789811498640121010l.

[3] S. Berlansky, M. Sallinger, H. Grabmayr, C. Humer, A. Bernhard, M. Fahrner, I. Frischauf, Calcium signals during SARS-CoV-2 infection: assessing the potential of emerging therapies, Cells 11 (2022) 253.

[4] https://www.worldometers.info/coronavirus/.

[5] C. Huang, Y. Wang, X. Li, L. Ren, J. Zhao, Y. Hu, L. Zhang, G. Fan, J. Xu, X. Gu, et al., Clinical features of patients infected with 2019 novel coronavirus in Wuhan, China, Lancet 395 (2020) 497–506, https://doi.org/10.1016/s0140-6736(20)30183-5.

[6] N.D. Yanez, N.S. Weiss, J.-A. Romand, M.M. Treggiari, COVID-19 mortality risk for older men and women, BMC Publ. Health 20 (2020) 1742, https://doi.org/10.1186/s12889-020-09826-8.

[7] W.-Y. Choi, Mortality rate of patients with COVID-19 based on underlying health conditions, 10.1017/dmp.2021.139, Disaster Med. Public Health Prep. (2021) 1–6, https://doi.org/10.1017/dmp.2021.139.

[8] A.A. Butt, S.R. Dargham, H. Chemaitelly, A. Al Khal, P. Tang, M.R. Hasan, P. V. Coyle, A.G. Thomas, A.M. Borham, E.G. Concepcion, et al., Severity of illness in persons infected with the SARS-CoV-2 delta variant vs beta variant in Qatar, JAMA Intern. Med. 182 (2022) 197–205, https://doi.org/10.1001/jamainternmed.2021.7949.

[9] S.K. Saxena, S. Kumar, S. Ansari, J.T. Paweska, V.K. Maurya, A.K. Tripathi, A. S. Abdel-Moneim, Characterization of the novel SARS-CoV-2 Omicron (B. 1.1. 529) variant of concern and its global perspective, J. Med. Virol. 94 (2022) 1738–1744, https://doi.org/10.1002/jmv.27524.

[10] F.P. Polack, S.J. Thomas, N. Kitchin, J. Absalon, A. Gurtman, S. Lockhart, J. L. Perez, G.P. Marc, E.D. Moreira, C. Zerbini, Safety and efficacy of the BNT162b2 mRNA Covid-19 vaccine, N. Engl. J. Med. 13 (2020) 2603–2615, https://doi.org/10.1056/NEJMoa2034577.

[11] L.R. Baden, H.M. El Sahly, B. Essink, K. Kotloff, S. Frey, R. Novak, D. Diemert, S. A. Spector, N. Rouphael, C.B. Creech, Efficacy and safety of the mRNA-1273 SARS-CoV-2 vaccine, N. Engl. J. Med. 384 (2020) 403–416, https://doi.org/10.1056/NEJMoa2035389.

[12] M. Voysey, S.A.C. Clemens, S.A. Madhi, L.Y. Weckx, P.M. Folegatti, P.K. Aley, B. Angus, V.L. Baillie, S.L. Barnabas, Q.E. Bhorat, Safety and efficacy of the ChAdOx1 nCoV-19 vaccine (AZD1222) against SARS-CoV-2: an interim analysis of four randomised controlled trials in Brazil, South Africa, and the UK, Lancet 397 (2021) 99–111, https://doi.org/10.1016/S0140-6736(20)32661-1.

[13] J. Sadoff, G. Gray, A. Vandebosch, V. Cárdenas, G. Shukarev, B. Grinsztejn, P. A. Goepfert, C. Truyers, H. Fennema, B. Spiessens, Safety and efficacy of single-dose Ad26. COV2. S vaccine against Covid-19, N. Engl. J. Med. 384 (2021) 2187–2201, https://doi.org/10.1056/NEJMoa2101544.

[14] R.L. Russell, P. Pelka, B.L. Mark, Frontrunners in the race to develop a SARS-CoV-2 vaccine, Can. J. Microbiol. 67 (2021) 189–212, https://doi.org/10.1139/cjm-2020-0465.

[15] G. Forni, A. Mantovani, COVID-19 vaccines: where we stand and challenges ahead, Cell Death Differ. 28 (2021) 626–639, https://doi.org/10.1038/s41418-020-00720-9.

[16] M. Abdalla, A.A. El-Arabey, X. Jiang, What are the challenges faced by COVID-19 vaccines? Expet Rev. Vaccine 21 (2022) 5–7, https://doi.org/10.1080/14760584.2022.2008245.

[17] S.S.A. Karim, Q.A. Karim, Omicron SARS-CoV-2 variant: a new chapter in the COVID-19 pandemic, Lancet 398 (2021) 2126–2128, https://doi.org/10.1016/S0140-6736(21)02758-6.

[18] R. Viana, S. Moyo, D.G. Amoako, H. Tegally, C. Scheepers, C.L. Althaus, U. J. Anyaneji, P.A. Bester, M.F. Boni, M. Chand, et al., Rapid epidemic expansion of the SARS-CoV-2 Omicron variant in southern Africa, 10.1038/s41586-022-04411-y, Nature (2022), https://doi.org/10.1038/s41586-022-04411-y.

[19] W.H.O.S.T. Consortium, H. Pan, R. Peto, A.M. Henao-Restrepo, M.P. Preziosi, V. Sathiyamoorthy, Q. Abdool Karim, M.M. Alejandria, C. Hernandez Garcia, M. P. Kieny, et al., Repurposed antiviral drugs for covid-19-interim WHO solidarity trial results, N. Engl. J. Med. 384 (2021) 497–511, https://doi.org/10.1056/NEJMoa2023184.

[20] M. Abdalla, A.A. El-Arabey, X. Jiang, Are the new SARS-CoV-2 variants resistant against the vaccine? Hum. Vaccines Immunother. 17 (2021) 3489–3490, https://doi.org/10.1080/21645515.2021.1925503.

[21] B. Ogunyemi, O. Oderinlo, In-silico investigation of oxoaporphine alkaloids of Xylopia aethiopica against SARS-COV-2 main protease, AROC Nat. Prod. Res. 2 (2022) 1–12, https://doi.org/10.53858/arocnpr02010112.

[22] D. Muhammed, B. Odey, B. Alozieuwa, R. Alawode, B. Okunlola, J. Ibrahim, A. Lawal, E. Berinyuy, Azadirachtin-A a bioactive compound from Azadirachta indica is a potential inhibitor of SARS-CoV-2 main protease, AROC Pharma. Biotechnol. 1 (2021) 1–8.

[23] M. Imran, M. Kumar Arora, S.M.B. Asdaq, S.A. Khan, S.I. Alaqel, M. K. Alshammari, M.M. Alshehri, A.S. Alshrari, A. Mateq Ali, A.M. Al-shammeri, et al., Discovery, development, and patent trends on molnupiravir: a prospective oral treatment for COVID-19, Molecules 26 (2021) 5795, https://doi.org/10.3390/molecules26195795.

[24] W.P. Painter, W. Holman, J.A. Bush, F. Almazedi, H. Malik, N.C.J.E. Eraut, M. J. Morin, L.J. Szewczyk, G.R. Painter, Human safety, tolerability, and pharmacokinetics of molnupiravir, a novel broad-spectrum oral antiviral agent with activity against SARS-CoV-2, Antimicrob. Agents Chemother. 65 (2021), https://doi.org/10.1128/AAC.02428-20 e02428–02420.

[25] V. Napolitano, A. Dabrowska, K. Schorpp, A. Mourão, E. Barreto-Duran, M. Benedyk, P. Botwina, S. Brandner, M. Bostock, Y. Chykunova, et al., Acriflavine, a clinically approved drug, inhibits SARS-CoV-2 and other betacoronaviruses, 10.1016/j.chembiol.2021.11.006, S2451-9456(2421)00513-00514,, Cell Chem. Biol. (2022), https://doi.org/10.1016/j.chembiol.2021.11.006.

[26] S. Pandamooz, B. Jurek, C.-P. Meinung, Z. Baharvand, A.S. Shahem-abadi, S. Haerteis, J.A. Miyan, J. Downing, M. Dianatpour, A. Borhani-Haghighi, et al., Experimental models of SARS-CoV-2 infection: possible platforms to study COVID-19 pathogenesis and potential treatments, Annu. Rev. Pharmacol. Toxicol. 62 (2022) 25–53, https://doi.org/10.1146/annurev-pharmtox-121120-012309.

[27] V. Sanna, S. Satta, T. Hsiai, M. Sechi, Development of targeted nanoparticles loaded with antiviral drugs for SARS-CoV-2 inhibition, Eur. J. Med. Chem. 231 (2022), 114121, https://doi.org/10.1016/j.ejmech.2022.114121.

[28] L. Menéndez-Arias, Decoding molnupiravir-induced mutagenesis in SARS-CoV-2, J. Biol. Chem. 297 (2021), https://doi.org/10.1016/j.jbc.2021.100867.

[29] Q. Yang, B. Li, J. Tang, X. Cui, Y. Wang, X. Li, J. Hu, Y. Chen, W. Xue, Y. Lou, et al., Consistent gene signature of schizophrenia identified by a novel feature selection strategy from comprehensive sets of transcriptomic data, Briefings Bioinf. 21 (2020) 1058–1068, https://doi.org/10.1093/bib/bbz049.

[30] S. Mostafavi, D. Ray, D. Warde-Farley, C. Grouios, Q. Morris, GeneMANIA: a real-time multiple association network integration algorithm for predicting gene function, Genome Biol. 9 (2008) S4, https://doi.org/10.1186/gb-2008-9-s1-s4.

[31] E.Y. Chen, C.M. Tan, Y. Kou, Q. Duan, Z. Wang, G.V. Meirelles, N.R. Clark, A. Ma'ayan, Enrichr: interactive and collaborative HTML5 gene list enrichment analysis tool, BMC Bioinf. 14 (2013) 128, https://doi.org/10.1186/1471-2105-14-128.

[32] M.V. Kuleshov, M.R. Jones, A.D. Rouillard, N.F. Fernandez, Q. Duan, Z. Wang, S. Koplev, S.L. Jenkins, K.M. Jagodnik, A. Lachmann, et al., Enrichr: a comprehensive gene set enrichment analysis web server 2016 update, Nucleic Acids Res. 44 (2016) W90–W97, https://doi.org/10.1093/nar/gkw377.

[33] E.A. Orellana, A.L. Kasinski, Sulforhodamine B (SRB) assay in cell culture to investigate cell proliferation, Bio Protocol. 6 (2016), e1984, https://doi.org/10.21769/BioProtoc.1984.

[34] B. Lawal, Y.-C. Kuo, A.T.H. Wu, H.-S. Huang, BC-N102 suppress breast cancer tumorigenesis by interfering with cell cycle regulatory proteins and hormonal signaling, and induction of time-course arrest of cell cycle at G1/G0 phase, Int. J. Biol. Sci. 17 (2021) 3224–3238, https://doi.org/10.7150/ijbs.62808.

[35] M.R. Boyd, K.D. Paull, Some practical considerations and applications of the National Cancer Institute in vitro anticancer drug discovery screen, Drug Dev. Res. 34 (1995) 91–109.

[36] B. Lawal, C.-Y. Lee, N. Mokgautsi, M.R. Sumitra, H. Khedkar, A.T.H. Wu, H.-S. Huang, mTOR/EGFR/iNOS/MAP2K1/FGFR/TGFB1 are druggable candidates for N-(2,4-Difluorophenyl)-2′,4′-Difluoro-4-Hydroxybiphenyl-3-Carboxamide (NSC765598), with consequent anticancer implications, Front. Oncol. *11* (2021), https://doi.org/10.3389/fonc.2021.656738.

[37] J.O. Olugbodi, O. David, E.N. Oketa, B. Lawal, B.J. Okoli, F. Mtunzi, Silver nanoparticles stimulates spermatogenesis impairments and hematological alterations in testis and epididymis of male rats, Molecules 25 (2020) 1063, https://doi.org/10.3390/molecules25051063.

[38] B. Lawal, O.K. Shittu, F.I. Oibiokpa, H. Mohammed, S.I. Umar, G.M. Haruna, Antimicrobial evaluation, acute and sub-acute toxicity studies of Allium sativum, J. Acute Dis. 5 (2016) 296–301, https://doi.org/10.1016/j.joad.2016.05.002.

[39] A. Hussain, S. Alshehri, M. Ramzan, O. Afzal, A.S.A. Altamimi, M.A. Alossaimi, Biocompatible solvent selection based on thermodynamic and computational solubility models, in-silico GastroPlus prediction, and cellular studies of ketoconazole for subcutaneous delivery, J. Drug Deliv. Sci. Technol. 65 (2021), 102699, https://doi.org/10.1016/j.jddst.2021.102699.

[40] H. Liu, L. Wang, M. Lv, R. Pei, P. Li, Z. Pei, Y. Wang, W. Su, X.-Q. Xie, AlzPlatform: an alzheimer's disease domain-specific chemogenomics knowledgebase for polypharmacology and target identification research, J. Chem. Inf. Model. 54 (2014) 1050–1060, https://doi.org/10.1021/ci500004h.

[41] W.M. Pardridge, CNS drug design based on principles of blood-brain barrier transport, J. Neurochem. 70 (1998) 1781–1792, https://doi.org/10.1046/j.1471-4159.1998.70051781.x.

[42] O. Trott, A.J. Olson, AutoDock Vina: improving the speed and accuracy of docking with a new scoring function, efficient optimization, and multithreading, J. Comput. Chem. 31 (2010) 455–461, https://doi.org/10.1002/jcc.21334.

[43] Marcus D. Hanwell, D.E. C, David C. Lonie, Tim Vandermeersch, Eva Zurek, Geoffrey R. Hutchison, Avogadro: an advanced semantic chemical editor, visualization, and analysis platform, J. Cheminf. 4 (2012) 17, https://doi.org/10.1186/1758-2946-4-17.

[44] V. Dalal, D. Golemi-Kotra, P. Kumar, Quantum mechanics/molecular mechanics studies on the catalytic mechanism of a novel esterase (FmtA) of Staphylococcus aureus, J. Chem. Inf. Model. 62 (2022) 2409–2420, https://doi.org/10.1021/acs.jcim.2c00057.
[45] P. Dhankhar, V. Dalal, J.K. Mahto, B.R. Gurjar, S. Tomar, A.K. Sharma, P. Kumar, Characterization of dye-decolorizing peroxidase from Bacillus subtilis, Arch. Biochem. Biophys. 693 (2020), 108590, https://doi.org/10.1016/j.abb.2020.108590.
[46] P. Dhankhar, V. Dalal, V. Singh, A.K. Sharma, P. Kumar, Structure of dye-decolorizing peroxidase from Bacillus subtilis in complex with veratryl alcohol, Int. J. Biol. Macromol. 193 (2021) 601–608, https://doi.org/10.1016/j.ijbiomac.2021.10.100.
[47] B. Lawal, Y.-L. Liu, N. Mokgautsi, H. Khedkar, M.R. Sumitra, A.T. Wu, H.-S. Huang, Pharmacoinformatics and preclinical studies of nsc765690 and nsc765599, potential stat3/cdk2/4/6 inhibitors with antitumor activities against nci60 human tumor cell lines, Biomedicines 9 (2021) 92, https://doi.org/10.3390/biomedicines9010092.
[48] B. Lawal, C.-Y. Lee, N. Mokgautsi, M.R. Sumitra, H. Khedkar, A.T. Wu, H.-S. Huang, mTOR/EGFR/iNOS/MAP2K1/FGFR/TGFB1 are druggable candidates for N-(2, 4-difluorophenyl)-2′, 4′-difluoro-4-hydroxybiphenyl-3-carboxamide (NSC765598), with consequent anticancer implications, Front. Oncol. 11 (2021) 656738, https://doi.org/10.3389/fonc.2021.656738.
[49] D.S. Visualizer, BIOVIA, Dassault Systèmes, BIOVIA Workbook, Release 2020; BIOVIA Pipeline Pilot, Release 2020, Dassault Systèmes, San Diego, 2020.
[50] D. Szklarczyk, A.L. Gable, D. Lyon, A. Junge, S. Wyder, J. Huerta-Cepas, M. Simonovic, N.T. Doncheva, J.H. Morris, P. Bork, et al., STRING v11: protein-protein association networks with increased coverage, supporting functional discovery in genome-wide experimental datasets, Nucleic Acids Res. 47 (2019) D607–d613, https://doi.org/10.1093/nar/gky1131.
[51] A.A. El-Arabey, M. Abdalla, In the face of the future, what do we learn from COVID-19? Hum. Vaccines Immunother. 17 (2021) 4119–4120, https://doi.org/10.1080/21645515.2021.1963174.
[52] B. Singh, J.A. Schwartz, C. Sandrock, S.M. Bellemore, E. Nikoopour, Modulation of autoimmune diseases by interleukin (IL)-17 producing regulatory T helper (Th17) cells, Indian J. Med. Res. 138 (2013) 591–594.
[53] D.J. Hartigan-O'Connor, L.A. Hirao, J.M. McCune, S. Dandekar, Th17 cells and regulatory T cells in elite control over HIV and SIV, Curr. Opin. HIV AIDS 6 (2011) 221–227, https://doi.org/10.1097/COH.0b013e32834577b3.
[54] M.D. Rosenblum, S.S. Way, A.K. Abbas, Regulatory T cell memory, Nat. Rev. Immunol. 16 (2016) 90–101, https://doi.org/10.1038/nri.2015.1.
[55] V. Golubovskaya, L. Wu, Different subsets of T cells, memory, effector functions, and CAR-T immunotherapy, Cancers 8 (2016) 36, https://doi.org/10.3390/cancers8030036.
[56] S.M. Kaech, E.J. Wherry, R. Ahmed, Effector and memory T-cell differentiation: implications for vaccine development, Nat. Rev. Immunol. 2 (2002) 251–262, https://doi.org/10.1038/nri778.
[57] N.N. Jarjour, D. Masopust, S.C. Jameson, T cell memory: understanding COVID-19, Immunity 54 (2021) 14–18, https://doi.org/10.1016/j.immuni.2020.12.009.
[58] J.I. Cohen, P.D. Burbelo, Reinfection with SARS-CoV-2: implications for vaccines, Clin. Infect. Dis. 73 (2021) e4223–e4228, https://doi.org/10.1093/cid/ciaa1866.
[59] J. Keehner, L.E. Horton, M.A. Pfeffer, C.A. Longhurst, R.T. Schooley, J.S. Currier, S.R. Abeles, F.J. Torriani, SARS-CoV-2 infection after vaccination in health care workers in California, N. Engl. J. Med. 384 (2021) 1774–1775, https://doi.org/10.1056/NEJMc2101927.
[60] C. Menni, K. Klaser, A. May, L. Polidori, J. Capdevila, P. Louca, C.H. Sudre, L. H. Nguyen, D.A. Drew, J. Merino, Vaccine side-effects and SARS-CoV-2 infection after vaccination in users of the COVID Symptom Study app in the UK: a prospective observational study, Lancet Infect. Dis. 21 (2021) 939–949.
[61] E.M. White, X. Yang, C. Blackman, R.A. Feifer, S. Gravenstein, V. Mor, Incident SARS-CoV-2 infection among mRNA-vaccinated and unvaccinated nursing home residents, N. Engl. J. Med. 385 (2021) 474–476.
[62] V.K. Jain, K.P. Iyengar, P. Ish, Elucidating causes of COVID-19 infection and related deaths after vaccination, Diabetes Metabol. Syndr.: Clin. Res. Rev. 15 (2021), 102212.
[63] S. Jasial, Y. Hu, J.r Bajorath, Assessing the growth of bioactive compounds and scaffolds over time: implications for lead discovery and scaffold hopping, J. Chem. Inf. Model. 56 (2016) 300–307.
[64] M. Orhan Puskullu, B. Tekiner, S. Suzen, Recent studies of antioxidant quinoline derivatives, Mini Rev. Med. Chem. 13 (2013) 365–372.
[65] K. Kaur, M. Jain, R.P. Reddy, R. Jain, Quinolines and structurally related heterocycles as antimalarials, Eur. J. Med. Chem. 45 (2010) 3245–3264.
[66] S. Mukherjee, M. Pal, Medicinal chemistry of quinolines as emerging anti-inflammatory agents: an overview, Curr. Med. Chem. 20 (2013) 4386–4410.
[67] S. Jain, V. Chandra, P.K. Jain, K. Pathak, D. Pathak, A. Vaidya, Comprehensive review on current developments of quinoline-based anticancer agents, Arab. J. Chem. 12 (2019) 4920–4946, https://doi.org/10.1016/j.arabjc.2016.10.009.
[68] A.E. Abdel-rahman, E.A. Bakhite, M.I. Abdel-Moneam, T.A. Mohamed, Synthesis and antibacterial activities of some new thieno-[2, 3-b] quinolines, Phosphorus, Sulfur, Silicon Relat. Elem. 75 (1993) 219–227.
[69] L. Senerovic, D. Opsenica, I. Moric, I. Aleksic, M. Spasić, B. Vasiljevic, Quinolines and quinolones as antibacterial, antifungal, anti-virulence, antiviral and anti-parasitic agents, Adv Exp Med Biol 1282 (2020) 37–69, https://doi.org/10.1007/5584_2019_428.
[70] R. Kaur, K. Kumar, Synthetic and medicinal perspective of quinolines as antiviral agents, Eur. J. Med. Chem. 215 (2021) 113220, https://doi.org/10.1016/j.ejmech.2021.113220.
[71] S. Kumar, S. Bawa, H. Gupta, Biological activities of quinoline derivatives, Mini Rev. Med. Chem. 9 (2009) 1648–1654, https://doi.org/10.2174/138955709791012247.
[72] S. Abd-Elsalam, E.S. Esmail, M. Khalaf, E.F. Abdo, M.A. Medhat, M.S. Abd El Ghafar, O.A. Ahmed, S. Soliman, G.N. Serangawy, M. Alboraie, Hydroxychloroquine in the treatment of COVID-19: a multicenter randomized controlled study, Am. J. Trop. Med. Hyg. 103 (2020) 1635–1639, https://doi.org/10.4269/ajtmh.20-0873.
[73] E. Manivannan, C. Karthikeyan, N.S.H.N. Moorthy, S.C. Chaturvedi, The rise and fall of chloroquine/hydroxychloroquine as compassionate therapy of COVID-19, Front. Pharmacol. *12* (2021), https://doi.org/10.3389/fphar.2021.584940.
[74] Z.-N. Lei, Z.-X. Wu, S. Dong, D.-H. Yang, L. Zhang, Z. Ke, C. Zou, Z.-S. Chen, Chloroquine and hydroxychloroquine in the treatment of malaria and repurposing in treating COVID-19, Pharmacol. Therapeut. 216 (2020), 107672, https://doi.org/10.1016/j.pharmthera.2020.107672.
[75] B. Mégarbane, J.-M. Scherrmann, Hydroxychloroquine and azithromycin to treat patients with COVID-19: both friends and foes? J. Clin. Pharmacol. 60 (2020) 808–814, https://doi.org/10.1002/jcph.1646.
[76] I. Yakoub-Agha, Hydroxychloroquine in Covid-19: does the end justify the means? Curr. Res. Trans. Med. 68 (2020) 81–82, https://doi.org/10.1016/j.retram.2020.04.002.
[77] E.A. Meyerowitz, A.G.L. Vannier, M.G.N. Friesen, S. Schoenfeld, J.A. Gelfand, M. V. Callahan, A.Y. Kim, P.M. Reeves, M.C. Poznansky, Rethinking the role of hydroxychloroquine in the treatment of COVID-19, Faseb. J. 34 (2020) 6027–6037, https://doi.org/10.1096/fj.202000919.
[78] O. Noureddine, N. Issaoui, O. Al-Dossary, DFT and molecular docking study of chloroquine derivatives as antiviral to coronavirus COVID-19, J. King Saud Univ. Sci. 33 (2021), 101248, https://doi.org/10.1016/j.jksus.2020.101248.
[79] S. Oh, J.H. Shin, E.J. Jang, H.Y. Won, H.K. Kim, M.G. Jeong, K.S. Kim, E. S. Hwang, Anti-inflammatory activity of chloroquine and amodiaquine through p21-mediated suppression of T cell proliferation and Th1 cell differentiation, Biochem. Biophys. Res. Commun. 474 (2016) 345–350, https://doi.org/10.1016/j.bbrc.2016.04.105.
[80] Y. Zhang, Y. Li, Y. Li, R. Li, Y. Ma, H. Wang, Y. Wang, Chloroquine inhibits MGC803 gastric cancer cell migration via the Toll-like receptor 9/nuclear factor kappa B signaling pathway, Mol. Med. Rep. 11 (2015) 1366–1371, https://doi.org/10.3892/mmr.2014.2839.
[81] A. Ramos-Avila, J.L. Ventura-Gallegos, A. Zentella-Dehesa, C. Machuca-Rodríguez, M.M. Moreno-Altamirano, V. Narváez, M. Legorreta-Herrera, Immunomodulatory role of chloroquine and pyrimethamine in Plasmodium yoelii 17XL infected mice, Scand. J. Immunol. 65 (2007) 54–62, https://doi.org/10.1111/j.1365-3083.2006.01869.x.
[82] S.T. Liew, L.X. Yang, Design, synthesis and development of novel camptothecin drugs, Curr. Pharmaceut. Des. 14 (2008) 1078–1097, https://doi.org/10.2174/138161208784246180.
[83] X. Ling, X. Liu, K. Zhong, N. Smith, J. Prey, F. Li, FL118, a novel camptothecin analogue, overcomes irinotecan and topotecan resistance in human tumor xenograft models, Am. J. Tourism Res. 7 (2015) 1765–1781.
[84] D. Guo, Y. Liu, T. Li, N. Wang, X. Zhai, C. Hu, P. Gong, Synthesis and antitumor activities of a new series of 4,5-dihydro-1H-thiochromeno[4,3-d]pyrimidine derivatives, Sci. China Chem. 55 (2012) 347–351, https://doi.org/10.1007/s11426-011-4477-6.
[85] P. Palanisamy, J. Jennifer, P. Muthiah, S. Kumaresan, Synthesis, characterization, antimicrobial, anticancer, and antituberculosis activity of some new pyrazole, isoxazole, pyrimidine and benzodiazepine derivatives containing thiochromeno and benzothiepino moieties, RSC Adv. 3 (2013), 19300, https://doi.org/10.1039/c3ra42283f.
[86] T.-C. Chen, C.-L. Wu, C.-C. Lee, C.-L. Chen, D.-S. Yu, H.-S. Huang, Structure-based hybridization, synthesis and biological evaluation of novel tetracyclic heterocyclic azathioxanthone analogues as potential antitumor agents, Eur. J. Med. Chem. 103 (2015) 615–627, https://doi.org/10.1016/j.ejmech.2014.09.050.
[87] H.-S. Huang, D.-S. Yu, T.-C. Chen, Thiochromeno [2, 3-c] quinolin-12-one derivatives, preparation method and application thereof, Google Patents (2015).
[88] H.-S. Huang, D.S. Yu, T.C. Chen, Novel thiochromeno [2, 3-c] quinolin-12-one derivatives, preparation method and application thereof, Appl. No: JP2014220347A (2015).
[89] B. Lawal, Y.-C. Wang, A.T.H. Wu, H.-S. Huang, Pro-Oncogenic c-Met/EGFR, Biomarker Signatures of the Tumor Microenvironment are Clinical and Therapy Response Prognosticators in Colorectal Cancer, and Therapeutic Targets of 3-Phenyl-2H-benzo[e][1,3]-Oxazine-2,4(3H)-Dione Derivatives, Front. Pharmacol. *12* (2021), https://doi.org/10.3389/fphar.2021.691234.
[90] B. Lawal, S. Sani, A.S. Onikanni, Y.O. Ibrahim, A.R. Agboola, H.Y. Lukman, F. Olawale, A.A. Jigam, G.E.-S. Batiha, S.B. Babalola, et al., Preclinical anti-inflammatory and antioxidant effects of Azanza garckeana in STZ-induced glycemic-impaired rats, and pharmacoinformatics of it major phytoconstituents, Biomed. Pharmacother. 152 (2022), 113196, https://doi.org/10.1016/j.biopha.2022.113196.
[91] J. De Leon, C.-J. Ruan, G. Schoretsanitis, C. De las Cuevas, A rational use of clozapine based on adverse drug reactions, pharmacokinetics, and clinical pharmacopsychology, Psychother. Psychosom. 89 (2020) 200–214, https://doi.org/10.1159/000507638.
[92] A.I. Nichols, K. Focht, Q. Jiang, S.H. Preskorn, C.P. Kane, Pharmacokinetics of venlafaxine extended release 75 mg and desvenlafaxine 50 mg in healthy CYP2D6 extensive and poor metabolizers, Clin. Drug Invest. 31 (2011) 155–167, https://doi.org/10.2165/11586630-000000000-00000.

[93] American Cancer Society, Cancer Facts & Figures 2021. Atlanta: American Cancer Society, 2021.
[94] M.L. Amin, P-Glycoprotein inhibition for optimal drug delivery, Drug Target Insights 7 (2013) 27–34, https://doi.org/10.4137/DTI.S12519.
[95] J. Robert, C. Jarry, Multidrug resistance reversal agents, J. Med. Chem. 46 (2003) 4805–4817, https://doi.org/10.1021/jm030183a.
[96] M. Bourrié, V. Meunier, Y. Berger, G. Fabre, Cytochrome P450 isoform inhibitors as a tool for the investigation of metabolic reactions catalyzed by human liver microsomes, J. Pharmacol. Exp. Therapeut. 277 (1996) 321–332.
[97] J.H. Lin, A.Y. Lu, Inhibition and induction of cytochrome P450 and the clinical implications, Clin. Pharmacokinet. 35 (1998) 361–390, https://doi.org/10.2165/00003088-199835050-00003.
[98] H. Hashimoto, K. Toide, R. Kitamura, M. Fujita, S. Tagawa, S. Itoh, T. Kamataki, Gene structure of CYP3A4, an adult-specific form of cytochrome P450 in human livers, and its transcriptional control, Eur. J. Biochem. 218 (1993) 585–595, https://doi.org/10.1111/j.1432-1033.1993.tb18412.x.
[99] K. Inoue, J. Inazawa, Y. Suzuki, T. Shimada, H. Yamazaki, F.P. Guengerich, T. Abe, Fluorescencein situ hybridization analysis of chromosomal localization of three human cytochrome P450 2C genes (CYP2C8, 2C9, and 2C10) at 10q24.1, Jpn. J. Hum. Genet. 39 (1994) 337–343, https://doi.org/10.1007/BF01874052.
[100] Y.-C. Yeh, B. Lawal, M. Hsiao, T.-H. Huang, C.-Y.F. Huang, Identification of NSP3 (SH2D3C) as a prognostic biomarker of tumor progression and immune evasion for lung cancer and evaluation of organosulfur compounds from allium sativum L. As therapeutic candidates, Biomedicines 9 (2021) 1582, https://doi.org/10.3390/biomedicines9111582.
[101] S.-Y. Wu, K.-C. Lin, B. Lawal, A.T.H. Wu, C.-Z. Wu, MXD3 as an onco-immunological biomarker encompassing the tumor microenvironment, disease staging, prognoses, and therapeutic responses in multiple cancer types, Comput. Struct. Biotechnol. J. 19 (2021) 4970–4983, https://doi.org/10.1016/j.csbj.2021.08.047.
[102] B. Lawal, A.T.H. Wu, H.-S. Huang, Leveraging bulk and single-cell RNA sequencing data of NSCLC tumor microenvironment and therapeutic potential of NLOC-15a, A novel multi-target small molecule, Front. Immunol. 13 (2022) 872470, https://doi.org/10.3389/fimmu.2022.872470.
[103] X.-Y. Meng, H.-X. Zhang, M. Mezei, M. Cui, Molecular docking: a powerful approach for structure-based drug discovery, Curr. Comput. Aided Drug Des. 7 (2011) 146–157, https://doi.org/10.2174/157340911795677602.
[104] D.B. Kitchen, H. Decornez, J.R. Furr, J. Bajorath, Docking and scoring in virtual screening for drug discovery: methods and applications, Nat. Rev. Drug Discov. 3 (2004) 935–949, https://doi.org/10.1038/nrd1549.
[105] J.-H. Chen, A.T.H. Wu, B. Lawal, D.T.W. Tzeng, J.-C. Lee, C.-L. Ho, T.-Y. Chao, Identification of cancer hub gene signatures associated with immune-suppressive tumor microenvironment and ovatodiolide as a potential cancer immunotherapeutic agent, Cancers 13 (2021) 3847, https://doi.org/10.3390/cancers13153847.
[106] B. Lawal, Y.-C. Kuo, S.-L. Tang, F.-C. Liu, A.T.H. Wu, H.-Y. Lin, H.-S. Huang, Transcriptomic-based identification of the immuno-oncogenic signature of cholangiocarcinoma for HLC-018 multi-target therapy exploration, Cells 10 (2021) 2873, https://doi.org/10.3390/cells10112873.
[107] B. Lawal, Y.-C. Kuo, M.R. Sumitra, A.T. Wu, H.-S. Huang, In vivo pharmacokinetic and anticancer studies of HH-N25, a selective inhibitor of topoisomerase I, and hormonal signaling for treating breast cancer, J. Inflamm. Res. 14 (2021) 1–13, https://doi.org/10.2147/JIR.S329401.